AGE ESTIMATES OF HOLOCENE GLACIAL RETREAT IN LAPEYRÈRE BAY, AN ANVERS ISLAND FJORD

A Thesis

Presented to

the Faculty of the Department of Earth and Atmospheric Sciences

University of Houston

In Partial Fulfillment

of the Requirements for the Degree

Master of Science

By

Kimberly Allison Mead

May 2012

AGE ESTIMATES OF HOLOCENE GLACIAL RETREAT
IN LAPEYRÈRE BAY, AN ANVERS ISLAND FJORD

Kimberly Allison Mead

APPROVED:

Dr. Julia Wellner, Co-Advisor
Research Assistant Professor
Department of Earth and Atmospheric Sciences

Dr. William Dupré, Co-Advisor
Associate Professor
Department of Earth and Atmospheric Sciences

Dr. Thomas Lapen
Associate Professor
Department of Earth and Atmospheric Sciences

Dr. Brad Rosenheim
Assistant Professor
Department of Earth and Environmental Sciences
Tulane University

Dean of the College of Natural Sciences and Mathematics

ACKNOWLEDGMENTS

My sincerest appreciation goes to Dr. Julia Wellner for her always-generous insight, encouragement, and guidance throughout the duration of this thesis. I also thank her for giving me the tremendous opportunity to take part in an Antarctic research cruise, an adventure that I will never forget. My thanks also go to Dr. William Dupré and Dr. Thomas Lapen for their time and technical support. This research was funded by the National Science Foundation, Office of Polar Programs grant OPP-0739596. Very special thanks to Dr. Brad Rosenheim for inviting me to spend a summer at the Tulane University Stable Isotope Laboratory and apply his chronology methods in this thesis. I also thank Dr. John Anderson and Dr. Adry Bissada for allowing me to their laboratories and equipment at Rice University and the University of Houston. I would also like to show my appreciation for Yuribia Muñoz, Laurin Hardin, Yanet Cuddus, Austin Luker, Dan Erklauer, and Alex Kirshner for their helpful feedback and support over the past two years.

AGE ESTIMATES OF HOLOCENE GLACIAL RETREAT
IN LAPEYRÈRE BAY, AN ANVERS ISLAND FJORD

An Abstract of a Thesis

Presented to

the Faculty of the Department of Earth and Atmospheric Sciences

University of Houston

In Partial Fulfillment

of the Requirements for the Degree

Master of Science

By

Kimberly Allison Mead

May 2012

ABSTRACT

Lapeyrère Bay is located on the eastern side of Anvers Island, off the Western Antarctic Peninsula. Though a large amount of data has been gathered in Lapeyrère Bay, very little has been published on the fjord's glacial retreat history. The primary purpose of this study is to reconstruct glacial retreat from Lapeyrère Bay using cores for chronology and facies analysis, shallow seismic for mapping facies, and multibeam swath bathymetry for identifying seafloor morphological features. Bathymetric maps display seafloor features including grounding zone wedges and a glacial outwash fan. Core data have documented five sediment facies, interpreted as open-marine, glacial outwash fan, and proximal glacial-marine deposits.

This study also seeks to assess the effectiveness of ramped pyrolysis, which dates individual fractions of organic material combusted at successively higher temperatures, by performing ramped pyrolysis ^{14}C dating and carbonate ^{14}C dating on the same cores. Nine carbonate ^{14}C dates and ramped pyrolysis ^{14}C dates from six depths in a proximal 20.3 m drill core yield discordant ages. Ramped pyrolysis ages are younger than carbonate ages, and the difference between both methods increases down-core. Ramped pyrolysis estimates the maximum age of the proximal core as ~4000 years younger than carbonate ^{14}C ages.

Two glacial reconstructions were developed to explain the deposition of older foraminifera with modern organic matter. The first scenario is a full deglaciation of Lapeyrère Bay ~14,000-8,500 cal yr BP followed by a re-advance of Iliad Glacier and unnamed glacier. During the subsequent retreat foraminifera, reworked by the glacial fluctuation, were deposited in the glacial outwash fan while modern organic matter fell

out of suspension. The second scenario is a full deglaciation between ~14,000-8,500 cal yr BP without subsequent re-advance. In this scenario foraminifera are reworked through turbidite flows and constant re-suspension prior to deposition.

The difference in dates yielded by ramped pyrolysis and carbonate ^{14}C methods may indicate the glacial retreat history of other Antarctic bays and fjords are more complex than previously recognized. The "gold standard" of dating Antarctic sediment cores, carbonate ^{14}C dating, may not be as reliable as previously thought.

CONTENTS

INTRODUCTION

The Antarctic Peninsula (AP) is one of the fastest warming regions on Earth, warming at an average rate of 3.4°C/century (Vaughan et al., 2003). In response, numerous studies are being conducted to document glacial retreat in the area (e.g. Cook et al., 2005; Rignot et al., 2008). But before interpreting the glacial response to modern warming and forecasting future melting trends, it is essential to put present changes in context with past ice retreat in the geologic record (Simms et al., 2011). After the Last Glacial Maximum (LGM), locally ~ 18,000 cal yr BP, ice that had been grounded at the continental shelf decoupled from the sea floor and retreated into AP bays and fjords as tidewater glaciers (Anderson et al., 2002; Fig. 1). The timing and direction of this retreat are constrained through seafloor morphological features (including glacial lineations, grounding zone wedges, and drumlins), which were carved into bedrock by receding ice (Wellner et al., 2006). Cores recovered by multiple cruises of the RV/IB *Nathaniel B. Palmer* also document retreat, through the transition from sub-glacial till to glacial-marine and open-marine sedimentary deposits. Using primarily seafloor morphology and sediment cores, this study seeks to place modern glacial retreat in context with the geologic record by documenting Holocene ice retreat in a single AP fjord: Lapeyrère Bay.

Lapeyrère Bay, like many AP fjords, lacks enough calcareous material for thorough carbonate radiocarbon (^{14}C) dating of cores. Establishing a clear and extensive age profile is essential when interpreting the timing of glacial retreat from sediment cores, therefore other methods of dating need to be tested. In addition to reconstructing the timing of glacial retreat from Lapeyrère Bay, this study seeks to assess the

effectiveness of a novel ^{14}C chronological method of dating: ramped pyrolysis. Ramped pyrolysis dates individual fractions of organic matter pyrolyzed at increasingly high temperatures.

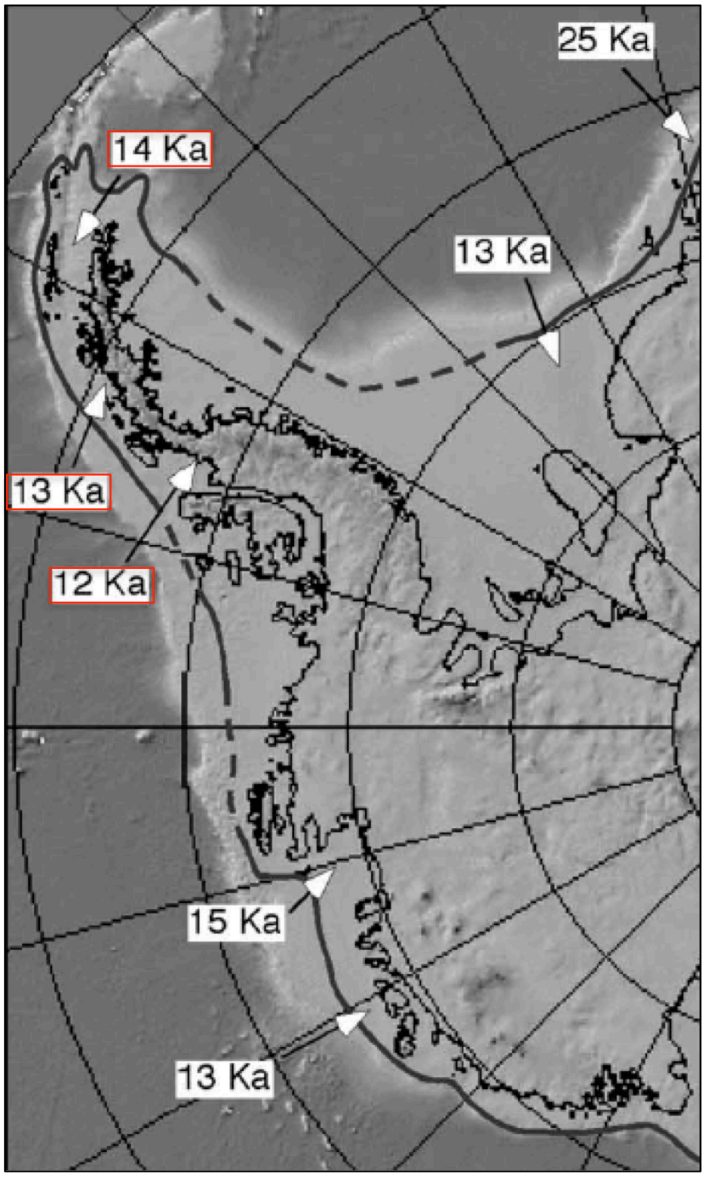

Figure 1. The maximum extent of grounded ice at the LGM, as indicated by the black line surrounding the Antarctic Peninsula and West Antarctica. Dates outlined in red represent the timing of glacial retreat from locations along the Antarctic Peninsula. Dates were acquired by ^{14}C dating sediments directly above sub-glacially deposited till in AP sediment cores (modified from Anderson et al., 2002).

BACKGROUND

Antarctic Ice Sheets

Antarctica is divided into three regions: the Antarctic Peninsula, West Antarctica, and East Antarctica. Vast ice sheets, the West Antarctic Ice Sheet (WAIS) and East Antarctic Ice Sheet (EAIS), overlie West Antarctica and East Antarctica, respectively. Unlike sea ice and ice shelves, which are already floating, ice sheets contain significant amounts of water that would dramatically impact sea level if melted. Together, the WAIS and EAIS amount to 25-30 x 10^6 km^3 of ice. If melted, the EAIS would result in 60 m of eustatic sea level rise, and the WAIS would result in 5 m of eustatic sea level rise (Bentley et al., 2009).

Currently, the EAIS is stable and grounded on the continent. However, the WAIS is grounded below sea level, and thus subject to destabilization by eustatic forcing. The WAIS also contains two floating ice shelves, the Ronne-Filchner and the Ross Ice Shelf. If these ice shelves were to disintegrate they would have no direct impact on sea level, but would no longer act as buttresses to the numerous West Antarctic glaciers behind them. The result would be a rapid increase in glacier flow rates, and thus sea-level rise (Scambos et al., 2003). This process of ice shelf disintegration followed by rapid glacier flow rates has been observed in the Antarctic Peninsula region following the 2002 breakup of the Larsen B ice shelf (Scambos et al., 2003). One of the first efforts to model WAIS and associated shelf disintegration was by Mercer (1978). He found a warming of 5°-10°C would result in a full breakdown of the WAIS (Fig. 2). More recent models agree that significant warming, ~5-7ºC would threaten the ice sheet as a result of

meltwater ponding (Joughin and Alley, 2011). Model predictions underlie the significance of understanding current and past ice responses to rapid warming.

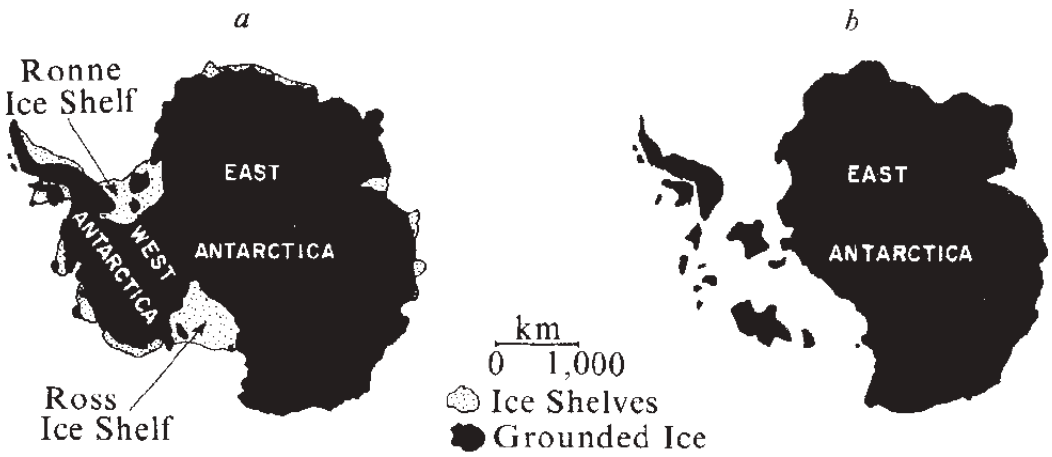

Figure 2. EAIS and WAIS depicted in black where grounded and white where floating ice shelves. *a*, describes Antarctica today, while *b*, is Antarctica after 5°-10°C of warming (Mercer, 1978).

Conversely, a significant grounded ice sheet does not overlie the AP. The AP ice volume of 95.2 x 10^3 km^3 is distributed between small glaciers on the western and eastern peninsula, and floating Larsen ice shelves on the eastern peninsula. If melted, this ice volume would not dramatically impact eustatic sea level, equivalent to 0.24 m of rise (Pritchard and Vaughan, 2007).

Modern Climate

Retaining ice in Antarctica is dependant on the sustained balance between ice loss through melting and calving, and ice formation through snow accumulation. This balance is directly tied to Antarctica's climate. The AP's warming climate, at a rate of 3.4°C/century, has increased precipitation (Vaughan et al., 2003). Warmer temperatures support snow accumulation through augmented moisture in the atmosphere, and by increasing the number of cyclones forming in the western Bellingshausen Sea (Vaughan

et al., 2003). At an average of 0.5-1.0 m of snow accumulation a year, the AP has the highest snow accumulation rate in Antarctica (Thomas et al., 2008). However, the increased precipitation is not balanced with modern AP ice loss. Modern accumulating snow does not have a long enough residence time to compact into ice, as the process of ice formation occurs on century to millennial time scales (Remy and Parrenin, 2004). Snow is likely melting and incorporating into glacial runoff prior to densification into ice, as the total number of positive degree-days in the AP has increased 74% since 1951 (Vaughan et al., 2003).

One result of the ice loss/accumulation imbalance in the AP is retreating glacial fronts. Cook and others (2005) documented the amount of AP glacial retreat since 1940 through satellite images and areal photographs. They found 212 of the region's 244 glacier fronts have retreated, with the boundary between advancing and retreating glaciers moving southward over time (Cook et al., 2005; Fig. 3). Another process initiated due to warming and contributing to deglaciation is known as "dynamic thinning," which is thinning through faster flow. Ice flow accelerated to 106-112% of 1993 flow rates, between 1993 and 2005 along the AP western coast. The increased flow velocities result in overall ice sheet thinning and ice mass loss (Pritchard and Vaughan, 2007; Pritchard et al., 2009).

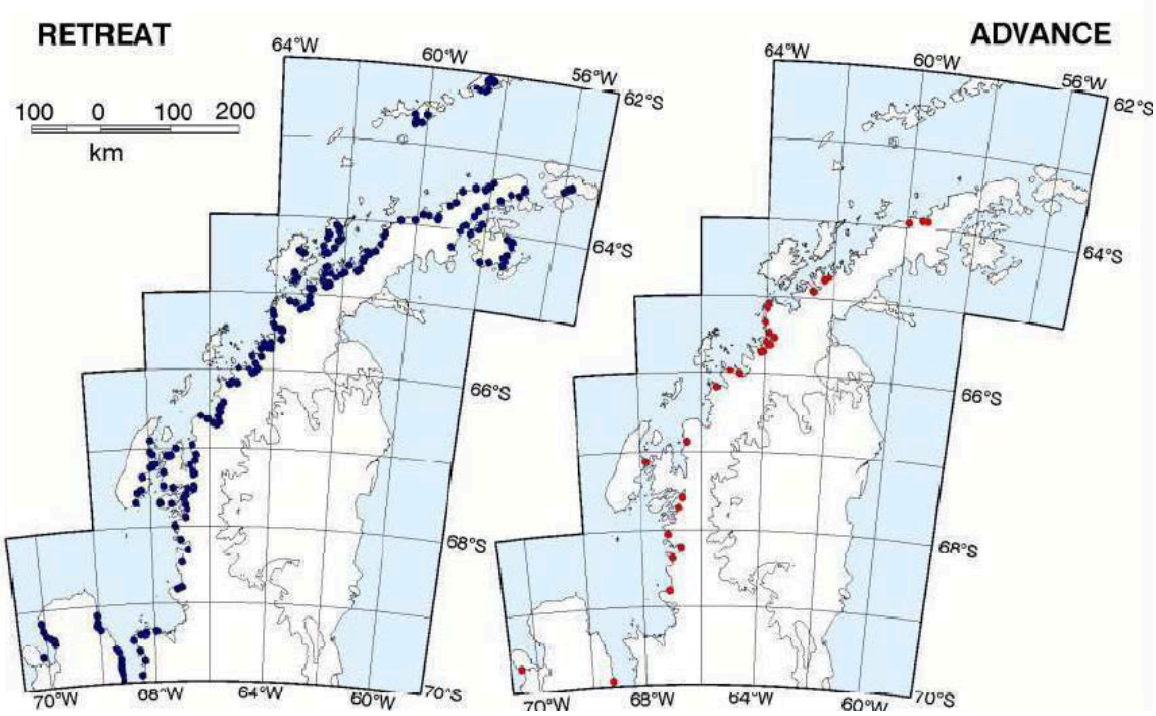

Figure 3. In blue, glaciers experiencing overall retreat since 1940 (212 glaciers). In red, glaciers experiencing overall advance since the 1940 (32 glaciers) (Cook et al., 2005).

Holocene Climate and Glacial History

Rapid ice retreat also occurred in the AP after the LGM. Heroy and Anderson (2007) used sedimentology and radiocarbon dating to constrain the timing and pattern of retreat from the continental shelf throughout the Holocene epoch. They found the ice shelf retreated from the outer shelf ~18,000 cal yr BP, and then continued through the middle and inner shelf areas ~14,000 cal yr BP. Deglaciation began in the northern AP and progressed southward (Heroy and Anderson, 2007). The rate of deglaciation changed throughout the Holocene, dependant on AP climate. Since the time that middle and inner ice shelf retreat commenced, four anomalously warm periods have been identified using ice and marine core paleoenvironmental proxies: the Early-Holocene Optimum (11,000-9,500 cal yr BP), the Mid Holocene Warm Period (4,500-2,800 cal yr BP), the Medieval

Warm Period (1,200-600 cal yr BP), and the Recent Rapid Warming (100 cal yr BP to present) (Bentley et al., 2009). Punctuating late Holocene warming events were cooling periods, which resulted in minor glacial re-advances (Heroy and Anderson, 2007). These periods include the Neoglacial (2,500-1,200 cal yr BP) and the Little Ice Age (700-150 cal yr BP) (Bentley et al., 2009; Fig. 4). Though environmental factors including air temperature, ocean current changes, and wind speed brought about these periods of warming and cooling they are recorded in sediment cores as changes in deposition rate, sediment composition and size distribution, and biogenic concentration.

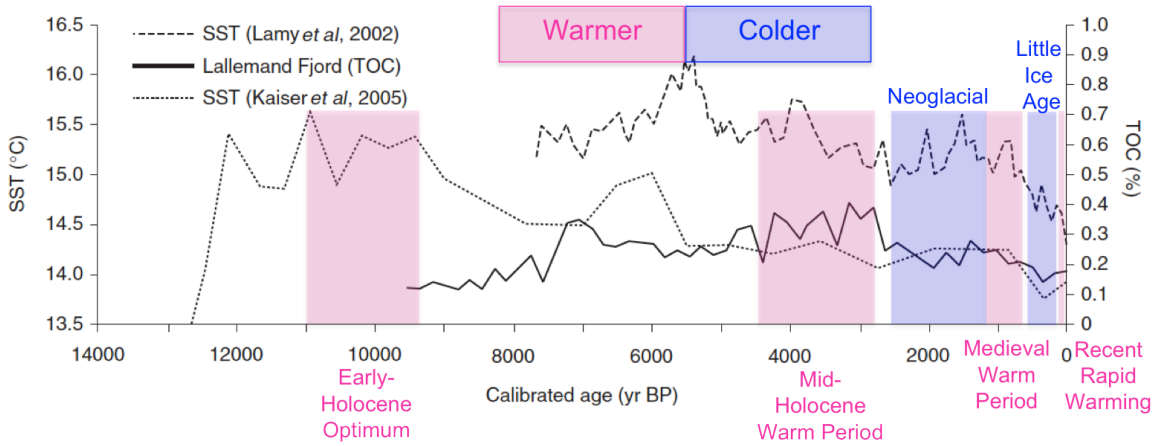

Figure 4. Periods of warming and cooling in the late Holocene determined by paleoenvironmental proxies (sea surface temperature and total organic carbon content) from AP ice and marine cores. Pink indicates periods of warming and blue indicates periods of cooling with minor glacial re-advances (Modified from Bentley et al., 2009; and references therein).

Glacial Sediments

The two primary components of glacial-marine deposits are biogenic particles and terrigenous sediments. Deposition of each was found to be highly seasonal in an AP sediment trap study by Khim and others (2007). Terrigenous sediments comprise 95% of total particle flux in the winter, and 88% in the summer. Fine-grained (clay-silt sized)

terrigenous sediment input during summer months is largely driven by the influx of snowmelt and glacial meltwater from nearby land, and therefore the snow accumulation rate from the previous winter. Biogenic particles in comparison are entirely dependant by the intensity of primary productivity of surface waters, and year-to-year variability of phytoplankton blooms (Khim et al., 2007). Organic particle content also varies with distance from the glacier front. Proximal to the glacier biogenics amount to 1% of sediment content, which increases distally to the mouth of the bay 1-2% in a study by Ashley and Smith (2000). They describe this trend as a result of dilution by meltwater near the glacier.

Terrigenous sediment is not only deposited through snowmelt runoff and glacial melt; grains are deposited through subglacial plumes and calved icebergs. After icebergs break off of tidewater glaciers, currents carry them away from their source. Through dropping, dumping, and grounding icebergs deposit ice rafted debris onto the seafloor. Dropping occurs when the base of an iceberg melts, allowing debris to sink to the seafloor. Dropping tends to produce dropstones and aggregated clasts. Dumping describes the overturning of an iceberg with a melted top. As the iceberg turns, exposed sediment on its surface slides into the water (Lonne, 1995). These dump deposits also appear coarse and poorly sorted. Grounding occurs when the iceberg makes contact with the seafloor, and disturbs sediment by dragging and ploughing. The results are scours and small craters (Lonne, 1995; and references therein). As these three processes involve the random melting of individual icebergs, ice rafted debris is discontinuously spaced on the seafloor. Around Anvers Island the debris is concentrated within 1 km from the glacial front, as most calved

icebergs melt within 1 km of the ice front due to tidal currents (Ashley and Smith, 2000).

Glacial sediments are also deposited through subglacial plumes. Meltwater at the base of the glacier erodes subglacial till or the underlying bedrock, and the eroded material is transported away from the glacier to be incorporated in seawater. This sedimentation model depends on specific hydrologic characteristics of the glacier, including enough pressure or geothermal melting to fully saturate till. Resulting outwash sediments may deposit to form fans or submarine deltas, and appear highly reworked and heterogeneous in grain size (Gustavson and Boothroyd, 1987).

Biogenic particles and terrigenous sediments (deposited by icebergs, surface and ice-front meltwater, and subglacial plumes) are recognizable in AP cores, and used to interpret glacial retreat. Variations in sediment composition record periods of proximal glacial-marine, distal glacial-marine, and open-marine settings. Trends used to identify these settings include an increasing pebble count, average grain-size, shear strength, and sedimentation rate more proximal to the glacier front. The percentage of the biogenic component increases distally (Domack and Ishman, 1993; Fernandez et al., 2011; Fig. 5).

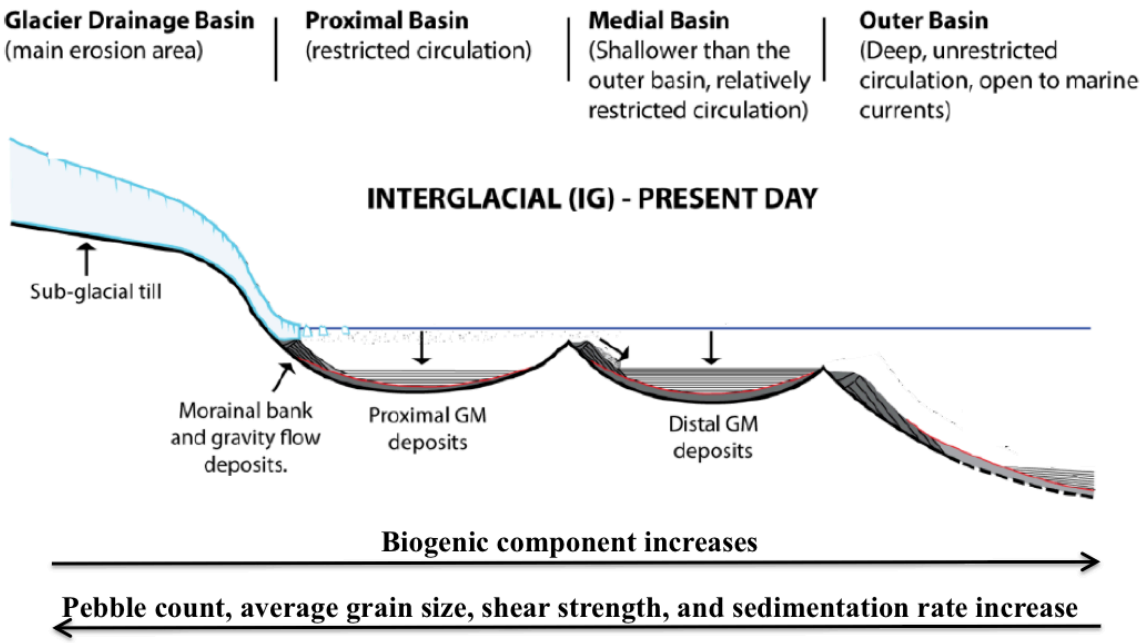

Figure 5. Trends used to identify proximal glacial-marine, distal glacial-marine, and open marine deposits in sediment cores. (Modified from Fernandez et al., 2011).

Antarctic Dating Methods

In order to determine the timing of glacial retreat from AP bay sediments, various chronology tools are needed to determine the age of facies changes within the sediments. A well-established method of dating is carbonate ^{14}C dating, which requires foraminiferal tests, shells, or other carbonate material to be extracted from the cores. In some AP fjord cores, and notably Lapeyrère Bay cores, finding enough calcareous material for thorough carbonate ^{14}C dating is a challenge. A number of studies have used bulk Acid Insoluble Organic Material (AIOM) to date sediments in Antarctic regions where carbonate cannot be found (e.g., Domack et al., 2001; Mosola and Anderson, 2006). However, this method often yields ages that are older than carbonate dates from the same horizon, which are interpreted to be closer to the true age (Leventer et al., 2006).

Ramped pyrolysis ^{14}C dating is a newer method, which may solve the AIOM problem of old ages by dating individual fractions of organic matter pyrolyzed at increasingly high temperatures (Rosenheim et al., 2008). The presumption is that the older, reworked, and diagenetically stable carbon is not combusted until higher temperatures are reached and thus minimizing the pre-aged contaminant in the gas formed at lower temperatures.

Study Area

Anvers Island is located on the western side of the AP, across the Gerlache Strait from the Danco Coast (Fig. 6). Anvers Island is 70 km long and 35 km wide, and is largely composed of coarse-grained granite (Rundle, 1973). The island has a maximum elevation (comprised of ice overlaying a mountain chain) of 2400 m, and experiences colder temperatures (-3°C annual average air temperature) and more precipitation (~1200 mm annual precipitation) than the South Shetlands which are ~230 km to the north (Ashley and Smith, 2000). Surface ice velocities are controlled largely by Anvers Island topography, with maximum velocities >200 m/yr found in bedrock valleys and minimum velocities 10-15 m/yr found between valleys (Rundle, 1973). On the eastern side of Anvers Island are two narrow fjords: Lapeyrère Bay and Fournier Bay (Fig. 7). The northern bay, Lapeyrère Bay, is the primary focus of this thesis (Fig. 8). A large glacier confined by steep walls and vulnerable to avalanching enters into Lapeyrère Bay. This valley glacier is named Iliad Glacier (Griffith and Anderson, 1989). To the north, a small-unnamed glacier feeds an unnamed cove, also known as Lapeyrère's thumb. The unnamed glacier is a

headland glacier, solely nourished by local accumulation (Griffith and Anderson, 1989; Fig. 9). Iliad Glacier is partly responsible for draining the ice cap of Anvers Island, as documented by ice flow patterns (Domack and Ishman, 1993). Though a large amount of data has been recently gathered by cruises in Lapeyrère Bay, very little has been published on the fjord's glacial retreat history or sediment flux.

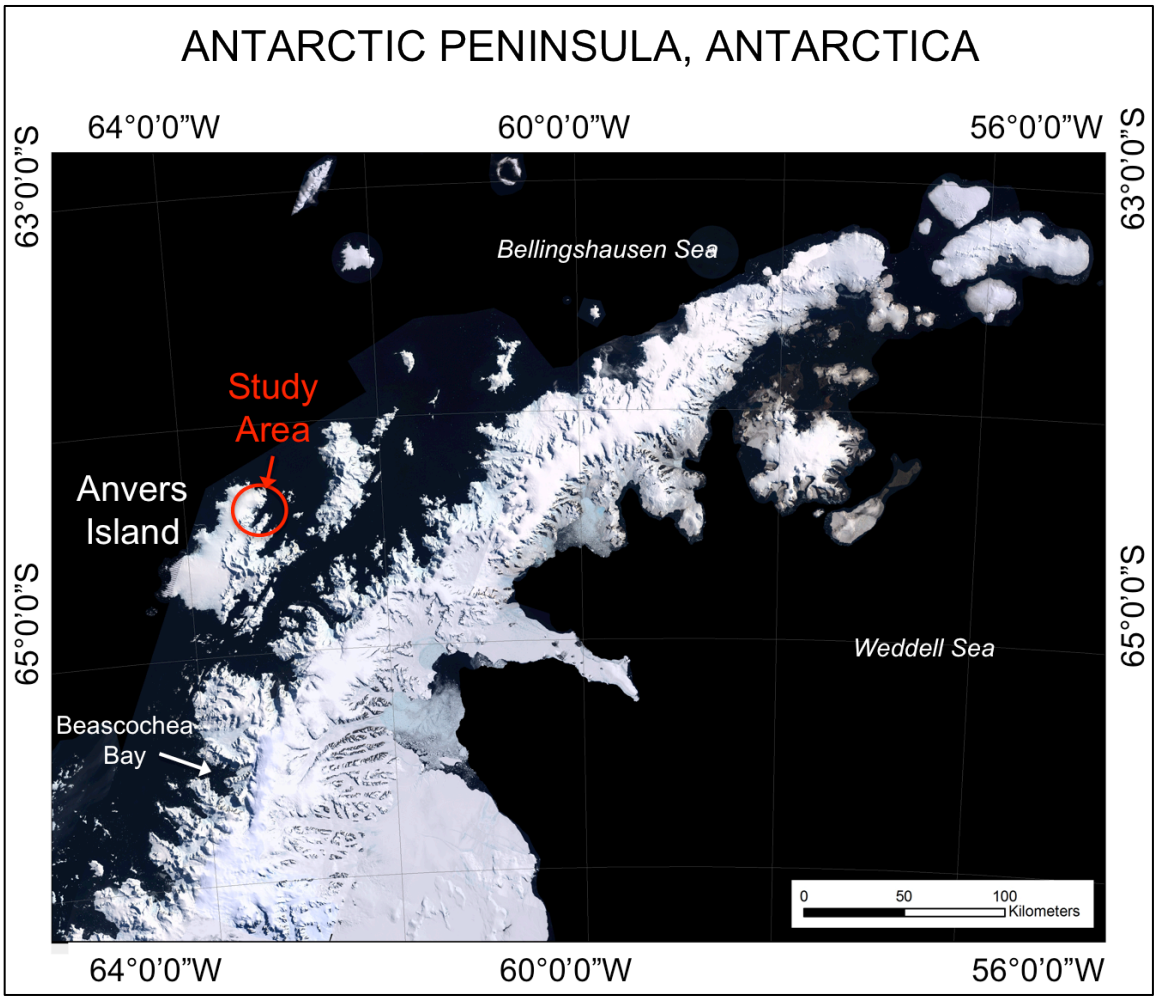

Figure 6. Image of the Antarctic Peninsula. Red circle indicates the study area on Anvers Island. Landsat Image Mosaic of Antarctica (LIMA) downloaded from http://lima.usgs.gov/access.php.

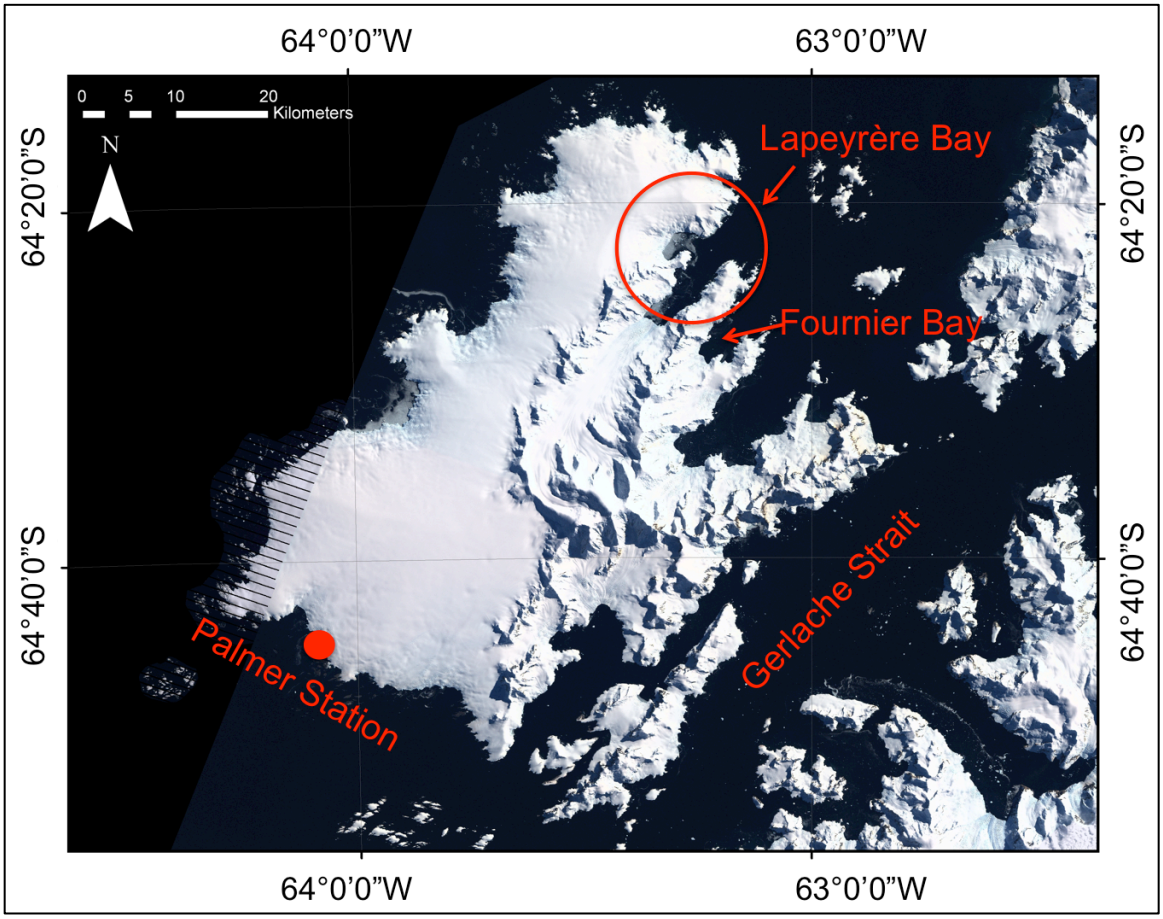

Figure 7. LIMA image of Anvers Island located off the Western Antarctic Peninsula. Red circle indicates the study area, Lapeyrère Bay.

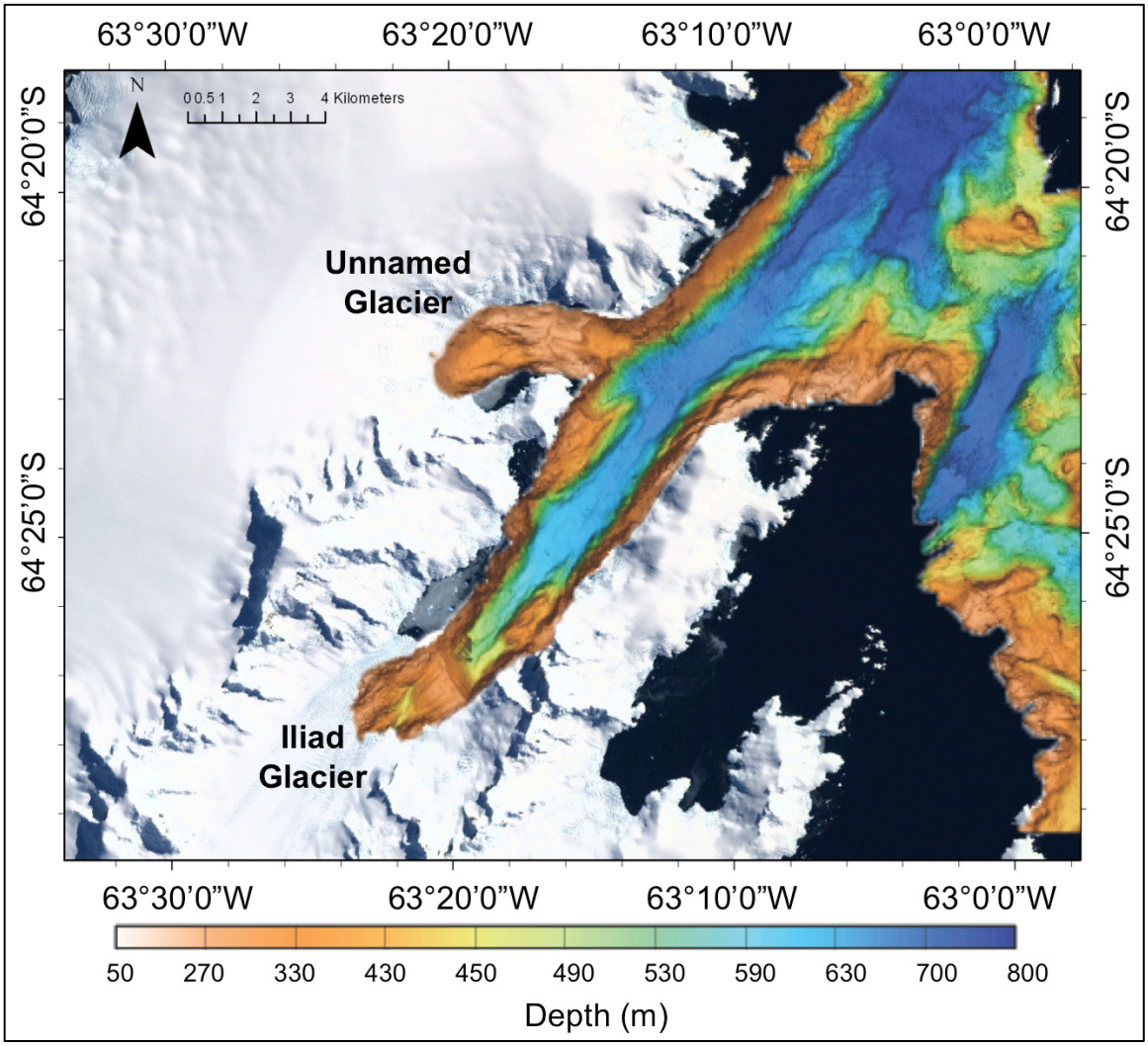

Figure 8. Lapeyrère Bay illustrated by LIMA and bathymetric data. Two glaciers enter Lapeyrère Bay, Iliad Glacier and an unnamed glacier.

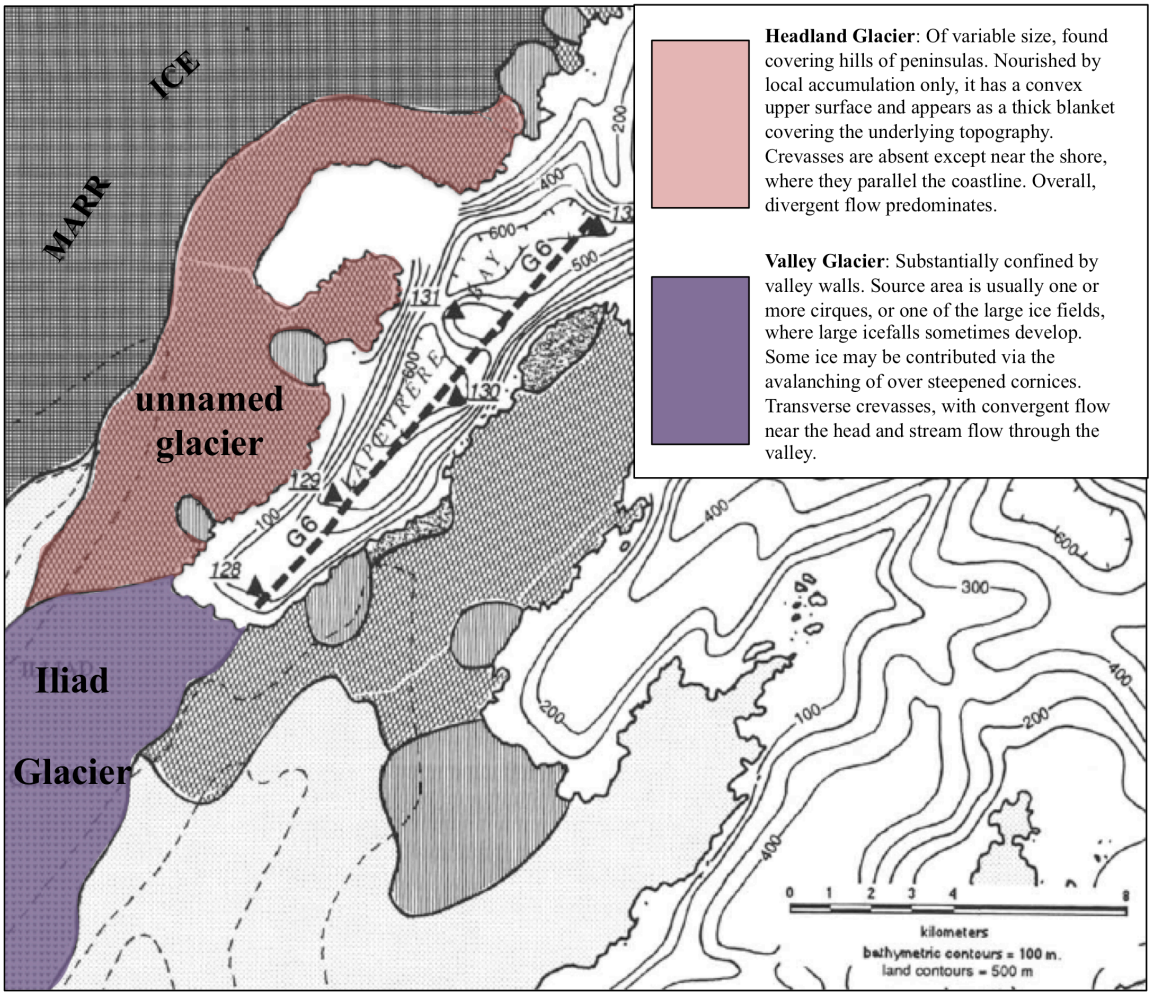

Figure 9. The Iliad Glacier, which feeds Lapeyrère Bay, is categorized as a valley glacier, and the small-unnamed glacier, which feeds the "thumb," as a headland glacier (Modified from Griffith and Anderson, 1989).

METHODS

Data used in this thesis were collected during two cruises of the RV/IB *Nathaniel B. Palmer* as part of a broader study of the Antarctic Peninsula. The first cruise was in 2005 (NBP0502, also called SHALDRIL I), and the second was in 2007 (NBP0703). Each cruise collected geophysical data, including multibeam swath bathymetry, and sediment cores in Lapeyrère Bay. In addition, a 1986 cruise of the USGS *Glacier* acquired air gun single channel seismic data in the proximal portion of Lapeyrère Bay.

This study focuses on two sediment cores, a rotary-drilled core and a jumbo piston core, and two radiometric isotopic dating methods, carbonate radiocarbon dating and ramped pyrolysis radiocarbon dating.

Multibeam Swath Bathymetry

A hull-mounted Simrad EM-120 was used to collect multibeam swath bathymetry data in Lapeyrère Bay. Acoustic signals were emitted from the base of the *Nathaniel B. Palmer* and the time between emission and reception was recorded. The time was then paired with GPS data to compile bathymetric maps. Using MB-System, the multibeam data were manually cleaned and gridded (10 x 10 m grid) onboard. Resulting high-resolution maps (a couple meters vertical resolution) allowed for the characterization of seafloor morphological features, which indicate the timing, speed, and direction of glacial retreat since in LGM.

Seismic

A single-channel air gun seismic survey from the 1986 United States Coast Guard icebreaker *Glacier* cruise was used in this study. The survey, number G6, crosses the proximal glacial outwash fan identified in multibeam, at the location of NBP0502 cores 6E and 6D.

Sediment Cores

This study focuses on two cores, a rotary-drilled core from the NBP0502 cruise (6E) and a jumbo piston core from the NBP0703 cruise (JPC-35), but incorporates observations from all cores taken in Lapeyrère Bay in 2005 and 2007 (Fig. 10). The NBP0502-6E core sampled the northern flank of Lapeyrère Bay, specifically an inner basin glacial outwash fan. The core was taken in 382 m of water, and collected 20.3 m of

material before encountering granite. A diamond drill bit was then used to recover 13 cm of the granite. Four other tightly clustered cores were attempted on the same fan. Of the four, only two kasten cores were successful, collecting 29 cm (KC-A) and 293 cm (KC-D) of sediment similar to that of the rotary-drilled core (Shipboard Scientific Party, 2005).

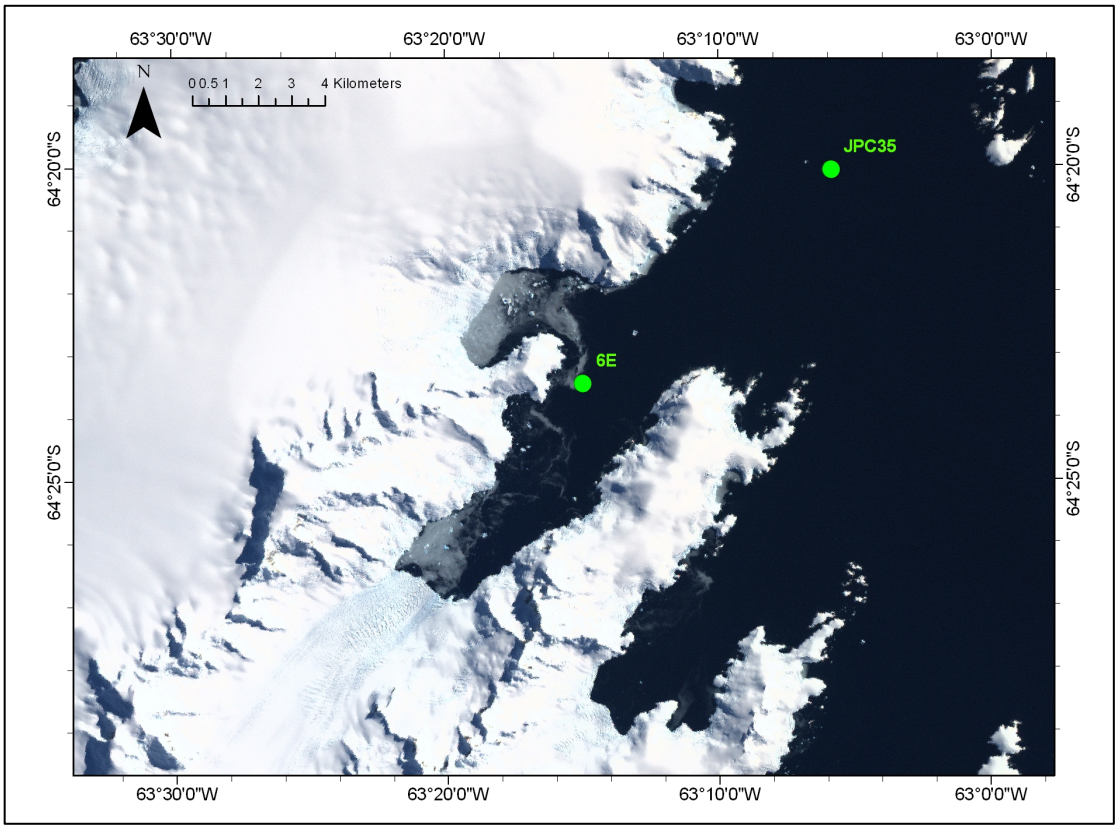

Figure 10. Lapeyrère Bay Locations of two primary cores utilized in the thesis, NBP0502 6E and NBP0703 JPC-35, as well as LIMA data. Note ice flow towards the bay from Iliad Glacier and an unnamed glacier.

The NBP0703 cruise recovered cores throughout Lapeyrère Bay. The core emphasized here, JPC-35, was collected from the outer basin and recovered 10.6 m of sediment in 769 m of water. A kasten core, KC-34, was taken adjacent to JPC-35 to ensure preservation of top sediment, as kasten cores collect sediment at the sediment-

water interface and jumbo piston cores usually do not recover the surface sediments. The kasten core collected 194 cm of sediment consistent with the upper most portion of JPC-35. In addition, the cruise collected one 289 cm core from the small-unnamed cove (KC-33), and attempted four cores in the middle of the basin. Three of the four middle basin cores were successful, the 303 cm KC-26, the 288 cm KC-28, and the 12.08 m JPC-37, and all resembled the proximal rotary drill core 6E from NBP0502 (Shipboard Scientific Party, 2007).

Cores were photographed and visually described immediately after collection and splitting. The visual descriptions included grain shape and size, texture, sedimentary structures, pebble lithology, evident macrofossils, and color using a Munsell color chart. These descriptions portray the original state of the core, prior to any deterioration during storage. Cores were stored at Florida State University's Antarctic Research Facility (ARF). All cores taken in Lapeyrère Bay by the NBP0502 and NBP0703 cruises were again described in March 2011, NBP0502 6E and NBP0703 JPC-35 under the most scrutiny. At ARF, cores were x-rayed to show any evidence of internal structures including laminations, bioturbation, ice rafted debris, and dropstones. Magnetic susceptibility, density, and resistivity measurements were also taken of the cores, using a Geotek™ multi-sensor core logger (MSCL); these MSCL measurements are used to determine compaction and the terrigenous versus biogenic component of the sediment. Smear slides were made for each horizon sampled for dating for evaluating changes in diatom abundance down core.

Rice University's Malvern Mastersizer 2000 Laser Particle Size Analysis (MLPSA) equipment was used to quantify grain-size. The MLPSA measured grains

between 0.02 and 2000 μm, while larger pebbles (>5 mm) were visually counted every 5 cm on x-rays. At ARF 5 cc samples were taken every 20 cm down-core for both NBP0502 6E and NBP0703 JPC-35. Sampling increased in frequency in areas of interest, including sand lenses. Samples were then combined with ~100 mL of de-ionized water and sodium metaphosphate to prevent clay flocculation. After samples were thoroughly stirred with magnetic stirrers and sat for ~24 hours, a portion of the mixture was extracted using a pipette and added to the MLPSA. When grain-size analysis was completed the data were characterized using the Wentworth grain-size classification with clay ranging from 0.02 to 4.0 μm, silt ranging from 4.0 to 63.0 μm, and sand ranging from 63.0 to 2000.0 μm (Wentworth, 1922).

Chronology

This study acted as an assessment of the effectiveness of ramped pyrolysis dating by conducting both ramped pyrolysis and carbonate ^{14}C dating on the NBP0502 6E and NBP0703 JPC-35 cores. Carbonate ^{14}C dates were acquired by wet-sieving core sediment samples with a 63 μm sieve to isolate fine terrigenous grains, foraminifera tests, and shell fragments (Fig. 11). After drying in an oven at ~50°C, a minimum of 1 mg of carbonate material was collected, bottled, and sent to the University of California, Irvine for ^{14}C-accelerator mass spectroscopy (AMS) processing. The resulting ages were corrected for the ^{14}C reservoir effect, the age of the dissolved inorganic carbon (DIC) used to precipitate $CaCO_3$ tests. The age of DIC is normally older than atmospheric CO_2 because of aging in the deepening ocean and mixing into the surface ocean. In this study ages were corrected for the old carbon reservoir effect using the 1100 BP correction for AP waters found by Milliken et al.

(2009). Ages were then calibrated to calendar years. Calendar year calibration was performed using CALIB 6.0 software Marine 09 calibration curve, which accounted for changes in ^{14}C levels in atmospheric CO_2 over time by dating tree rings (Stuiver and Reimer, 1993). Nine carbonate ^{14}C dates were acquired from the inner fjord, five from NBP0502 6E and four from adjacent KC-6D, which is from the same location as NBP0502 6E. Only two dates were acquired for NBP0703 JPC-35, due to a particular lack of foraminifera.

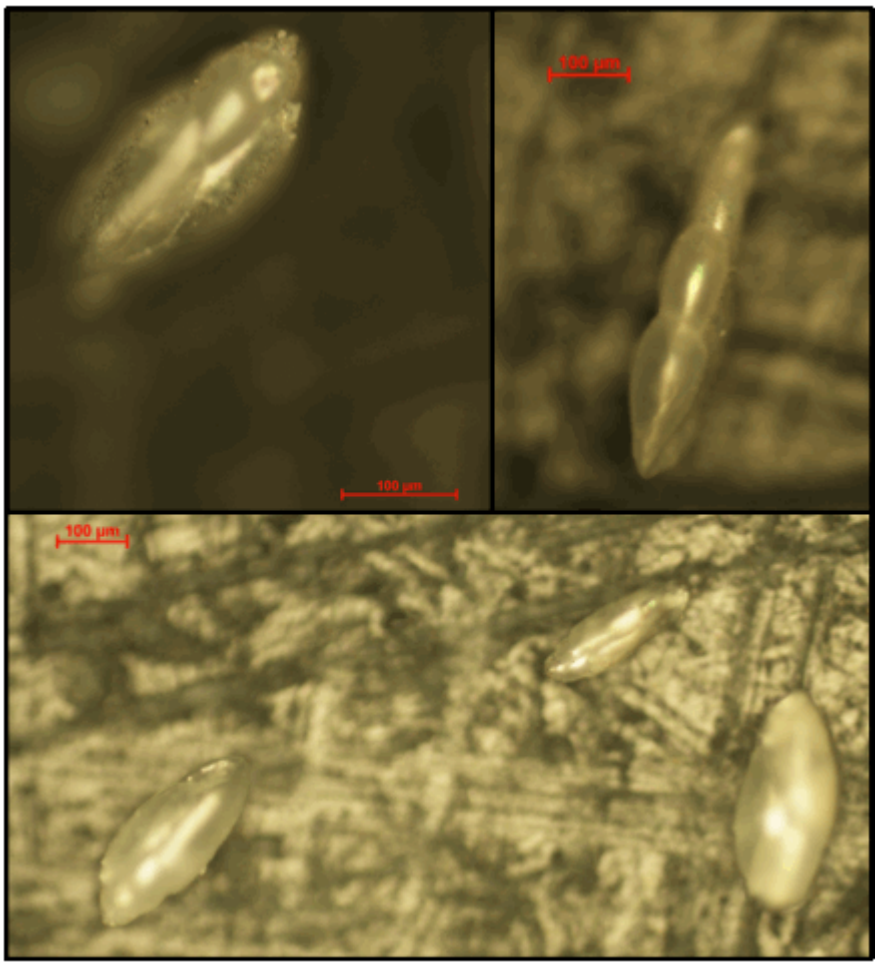

Figure 11. Foraminifera collected from sample NBP0502 6E-2E-2 horizon 230-235cm. The red line indicates 100 µm. Upper left and bottom foraminifera identified as *Fursenkoina fusiformis.* Upper right foraminifera identified as *Stainforthia corplanata* (Ishman, S., per. com.).

The second ^{14}C dating method applied was ramped pyrolysis. Ramped pyrolysis was conducted on nine samples, six in NBP0502 6E and three in NBP0703 JPC-35. Sample preparation was done at Tulane University's Stable Isotope Laboratory, using the methods of Rosenheim et al. (2008). To prepare samples for ramped pyrolysis dating, sediments were dried in an oven at ~50°C and ground by hand. The pulverized samples were added to glass centrifuge vials and acid washed with 2N HCL. Vials remained undisturbed for ~30 minutes and then were centrifuged for ~10 minutes to dissolve all calcareous material. After, water was added to each sample and centrifuging continued until mixtures were thoroughly combined. All liquid was then removed and samples were pH tested. This rinsing process was repeated until all samples neared a pH of 7, at which point they were placed in an oven at ~60°C for 24 hours. To prevent radiocarbon contamination gloves were worn while handling samples and tools were regularly washed with methanol. Plastics were not used in the laboratory, as they represent possible contamination of carbon.

Before beginning ramped pyrolysis dating, all nine samples were analyzed for total organic carbon (TOC) content. TOC was necessary to determine the amount of sediment needed for each sample to produce approximately 100 μmol of CO_2 gas. The laboratory's Vario MicroCube Elemental Analyzer (EA) measured TOC from 10 mg of acid-washed sediment. TOC measurements were also acquired at Dr. Adry Bissada's lab at the University of Houston using similar methods. TOC measurements were different from each lab, though consistently offset. Data

gathered from the EA at Tulane were chosen for ramped pyrolysis preparation, as both methods would be performed on exactly the same samples, pretreated at the same time.

Next, each sample's weight equivalent of 100 μmol of CO_2 was measured onto pre-combusted quartz wool and inserted into a quartz reaction tube. The tube was then placed in the pyrolysis furnace and gradually heated from ambient temperatures to ~800°C through a temperature ramp of +5°C/min. Emitted gasses were trapped in one of two active-trapping 9-loop traps immersed in liquid nitrogen (-195°C). At any one time, the other trap was open to a vacuum line for evacuation or sample transfer. The traps were toggled when enough CO_2 had accumulated (estimated from an infrared gas analyzer) or when the reaction had an inflection point of interest. Once transferred to the vacuum line, samples were cryogenically separated through a series of two 4-loop traps immersed alternatively in an isopropyl alcohol slush and liquid N_2 to trap water and CO_2 respectively (Fig. 12). Five samples of CO_2 gas (ranging from ~8 to 28 μmol CO_2 as quantified in a known volume) were collected for each pyrolysis run of a sediment sample. The gas samples (aliquots) were flame sealed in Pyrex vials with cupric oxide and silver granules, and again combusted at 525°C for 2 hours to remove any sulfur compounds that could potentially adversely affect graphitization for ^{14}C analysis. After being transported to the Woods Hole Oceanographic Institution samples were dated using ^{14}C and $\delta^{13}C$ analysis. Five aliquots were collected for each sediment sample pyrolysis run to show an increase in age with temperature, as fresh and less

diagenetically stable autochthonous organic debris is typically combusted first (Rosenheim et al., 2008; Fig. 13).

Figure 12. The Stable Isotope Laboratory at Tulane University. After organic mater was combusted it was passed through the vacuum line shown here. Water and noncondensible gases were cryogenically removed using a cooled isopropyl and liquid N_2 in insulated dewars (blue canisters).

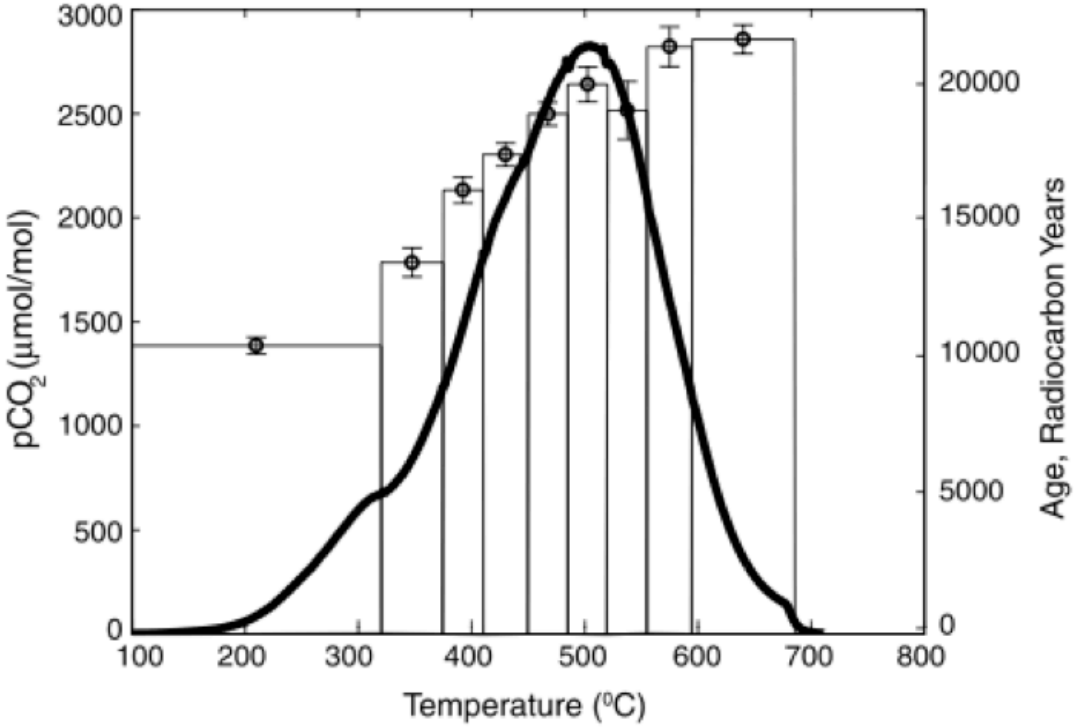

Figure 13. Thermograph from previous ramped pyrolysis study (on cores from the NW Weddell Sea, Eastern Antarctic Peninsula), in which ramped pyrolysis was compared to AIOM dating. No carbonate material was dated from this core. Bar height indicates age of aliquot trapped over a temperature range (bar width). Photometrically measured CO_2 is also noted on the left axis as measured on the heavy black line. The aliquot captured between ambient and 320°C, containing 11.5 µmol CO_2, is the "true age" of the sample as it is the youngest (10,400 ^{14}C years). A plateau is also apparent, representing the final combustion of fresh autochthonous organic material and the maximum age of the sample (Rosenheim et al., 2008).

Differing from previous studies of ramped pyrolysis, this thesis calibrated and reservoir corrected ramped pyrolysis ages using the same methods as the carbonate ^{14}C dates. This allowed both methods of dating to be directly compared, and facies to be described and visualized in terms of calendar years before present (cal yr BP). Calibration and reservoir correction of ramped pyrolysis data was appropriate, as the organic matter dated formed in the same carbon environment as the calcareous foraminifera tests.

DATA AND RESULTS

Multibeam Swath Bathymetry Data

Multibeam swath bathymetry has been collected for the entire seafloor of Lapeyrère Bay. The deepest part of the outer bay, where NBP0703 JPC-35 was cored, averages ~700 m water depths, whereas the deepest part of the inner bay averages ~500 m water depths. This indicates Lapeyrère Bay is a very gently sloping feature, sloping ~0.8°. Multibeam also revealed both Iliad Glacier and the unnamed glacier enter the bay in ~200 m water depths, demonstrating a ~300 m thick sediment buildup at both glacial terminuses. Additionally, multibeam depicted the steeply (~30°) sloping walls of Lapeyrère Bay, which classify the bay as a fjord.

Multibeam data also exposed distinct morphological features on the seafloor. Because grounding at the continental shelf during the LGM, locally ~14,000 cal yr BP, glaciers retreated to their current positions (Anderson et al., 2002). During this retreat glaciers scraped all unconsolidated material off the seafloor, leaving bare bedrock and morphological features documenting the retreat (Heroy and Anderson 2005; Fig. 14).

These features have been recorded on a large scale for the entire AP, and were found on a smaller scale in Lapeyrère Bay.

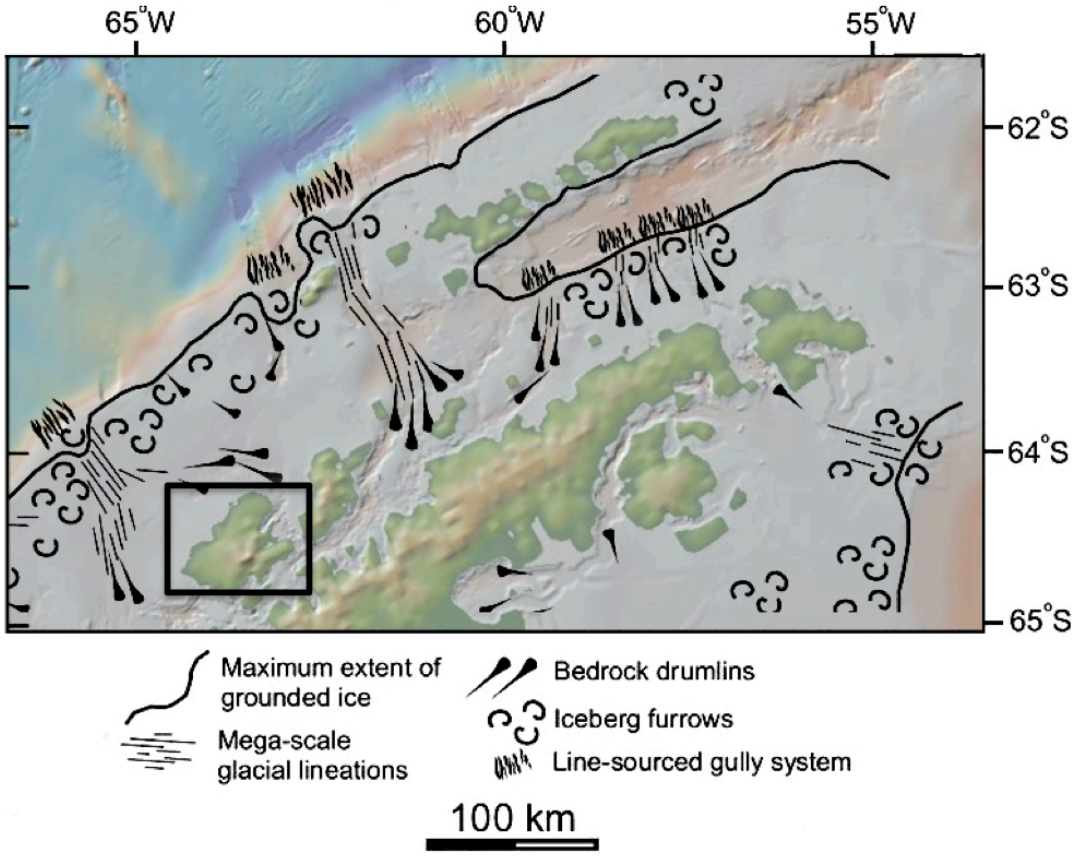

Figure 14. Large-scale geomorphic features around the AP documenting grounded ice retreat since the LGM. Study area, Anvers Island, boxed in black (Barnard, 2010).

Two features were particularly apparent: grounding zone wedges and a glacial outwash fan. Grounding zone wedges are large build-ups of glacial-marine sediment and till. These sediment piles are formed when glaciers pause or switch from a period of advancing to retreating (Wellner et al., 2001). Three grounding zone wedges were found in Lapeyrère Bay indicative of two pauses in glacial flow. The outer most grounding zone wedge (Fig. 15C) is less sharp compared to the proximal two, and deeper. This is due to several processes related to its age: erosion by meltwater, furrowing by icebergs calved

from Iliad and unnamed glaciers, and draping by open marine sediments. After the outer most grounding zone wedge was deposited, Iliad Glacier and the unnamed glacier resumed retreat and deposited the two very clear and proximal grounding zone wedges (Fig.15A and B). Both wedges are non-reworked and similarly positioned near the ocean interface of their respective tidewater glaciers. The grounding zone wedge at the terminus of Iliad Glacier is particularly well defined, as it is steeply sloped and crested by parallel lineations.

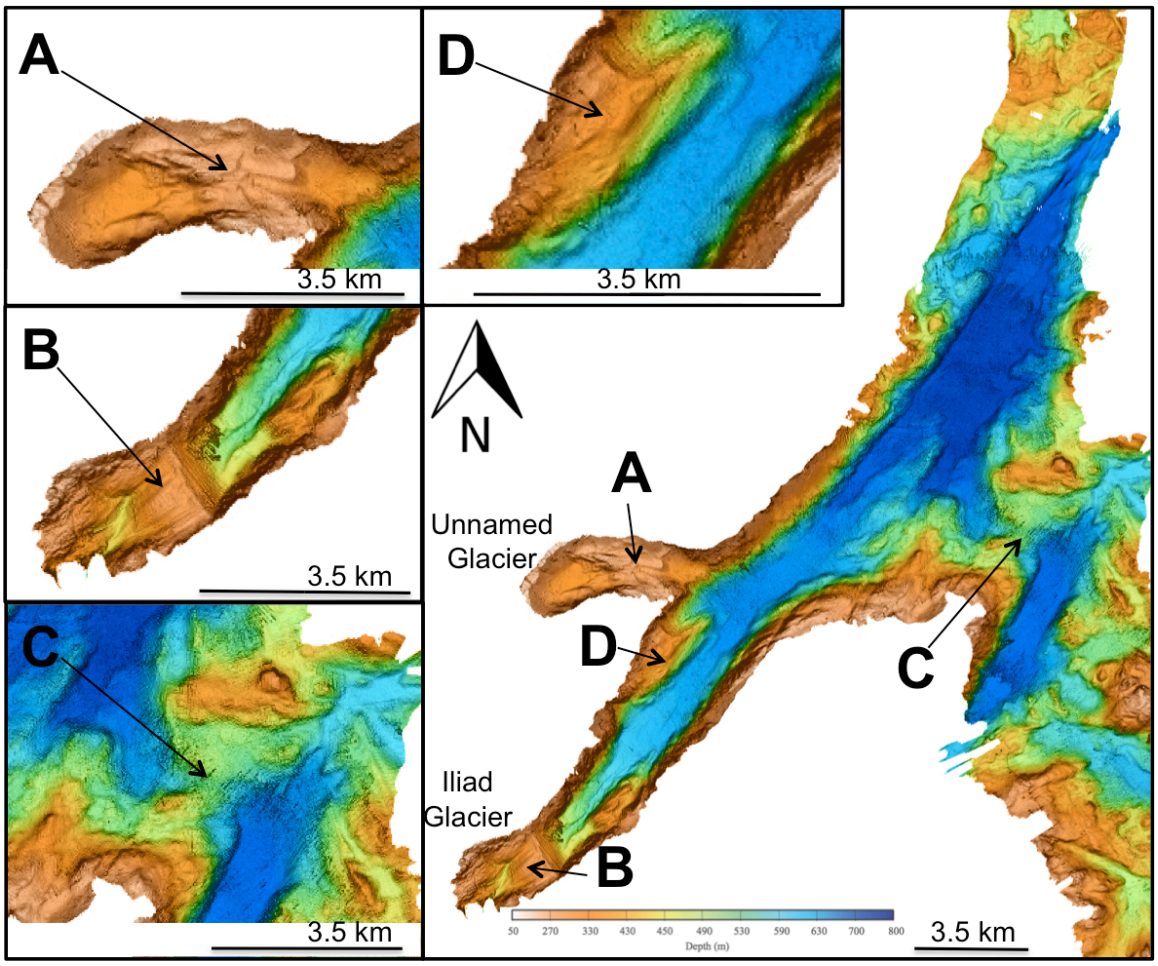

Figure 15. Geomorphic features found in multibeam data indicative of glacial retreat from Lapeyrère Bay. (A) Grounding zone wedge most recently deposited by unnamed glacier. (B) Recent grounding zone wedge deposited by Iliad Glacier. (C) Older reworked grounding zone wedge. (D) Glacial outwash fan deposited by sediment laden hypopycnal plumes.

The other geomorphic feature identified by multibeam data was a glacial outwash fan (Fig. 15D). The fan is in the proximal fjord, and was likely built by sediment-laden hypopycnal plumes originating at Iliad Glacier. Pressure melting at the base of Iliad Glacial formed meltwater, which fully saturated till deposits. The meltwater, carrying eroded sediments from the grounding zone, transported the load into the open fjord. Once at the ocean, the sediment-freshwater mixture was less dense than the seawater, and

therefore rose to the top of the water column. The plume transported sediment a distance from the glacier prior to the debris falling out of suspension and depositing as the outwash fan (Gustavson and Boothroyd, 1987; Domack and Ishman, 1993; Fig. 16).

A sediment-laden surface plume was seen emanating from Iliad Glacier during a two-helicopter survey on the 1986 *Glacier* cruise to Lapeyrère Bay. This sediment-laden surface plume is consistent with what is commonly found adjacent to tidewater glaciers in modern day AP fjords (Griffith and Anderson, 1989). Two hypopycnal plumes were found at the terminus of Maar glacier, on the southwestern side of Anvers Island, containing as much as 35 mg of sediment per liter of water (Ashley and Smith, 2000). Similar plumes, described as "cold tongues," were found in Andvord Bay directly across the Gerlache Straight from Anvers Island (Domack and Ishman, 1993). The glacial outwash fan is in part identified as a fan and not a slump deposit from the northern fjord wall because it is a time-progressive feature. Dates (both carbonate and ramped pyrolysis ^{14}C methods) from core NBP0502 6E, drilled through the fan, are in chronological order (Fig. 10).

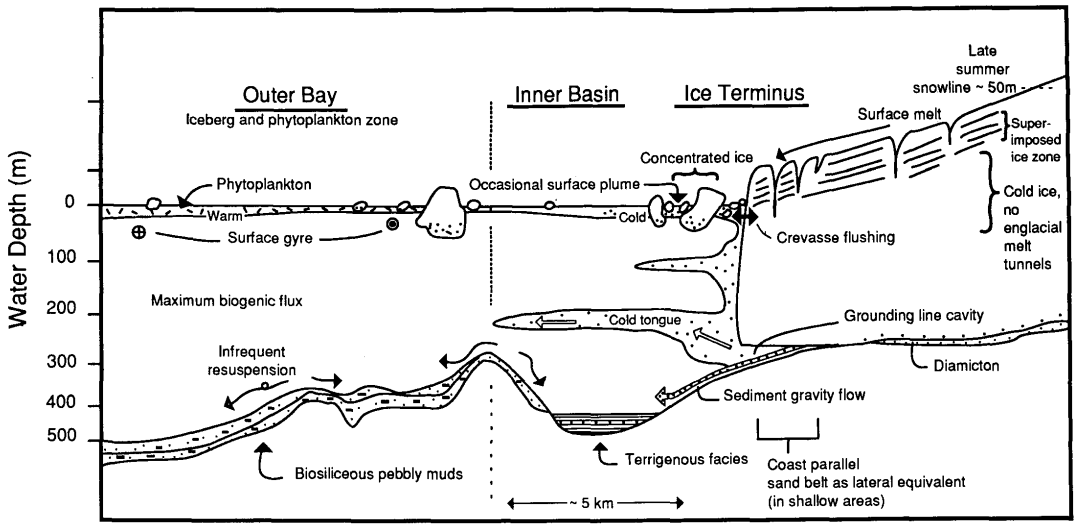

Figure 16. Schematic of basal meltwater and sediment-laden plume production in fjords along the Danco Coast (Domack and Ishman, 1993).

Seismic Data

An air gun seismic survey conducted in Lapeyrère Bay on the *Glacier* 1986 cruise documented the inner fjord, including the glacial outwash fan location of core NBP0502 6E (Fig. 17). The survey clearly identified the acoustic basement, as dense substrate returned very hard reflections (Fig. 18). This acoustic basement is interpreted as subglacial till or crystalline basement, and appears to be shallowest at the ice front (recent grounding zone wedge deposit) and beneath the glacial outwash fan deposit. Onlapping the acoustic basement are sediment drapes. The sediment drape between the ice front and glacial outwash fan is ~ 40 m thick, while the drape at the NBP0502 6E core location is ~ 25 m thick. The bottom of the drilled NBP0502 6E core collected 13 cm of granite. This granite likely originated from a large boulder in the Iliad subglacial till deposit, and therefore the core barely permeated the acoustic basement. The final sediment drape identified in the seismic line is between the glacial outwash fan and the outer fjord. The drape is ~ 20 m thick.

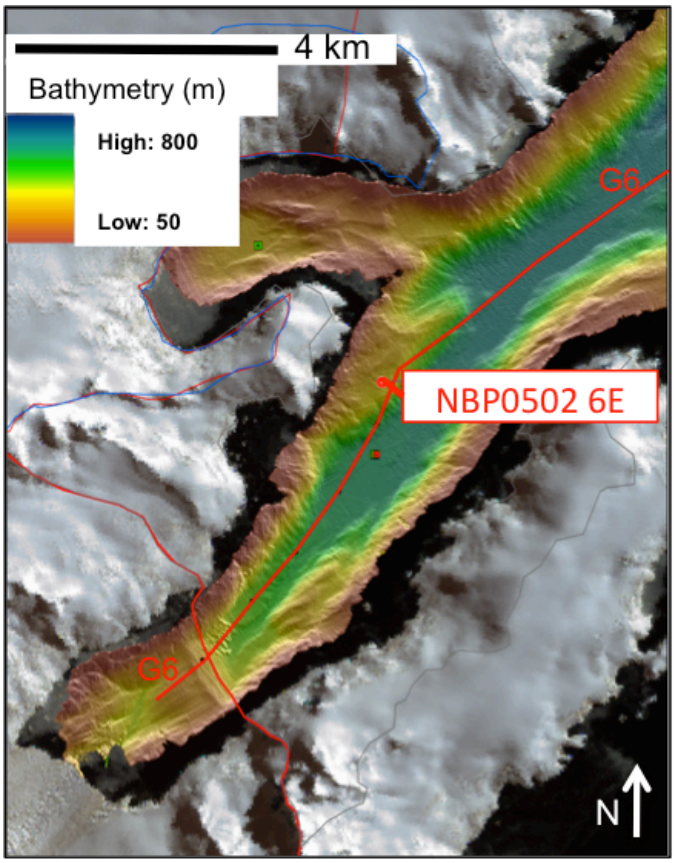

Figure 17. Bathymetry of Lapeyrère Bay with the location of seismic line G6 annotated in red. The line documents the interior of the inner bay, as well of the glacial outwash fan deposit and core NBP0502 6E (Fernandez, R., per. com.).

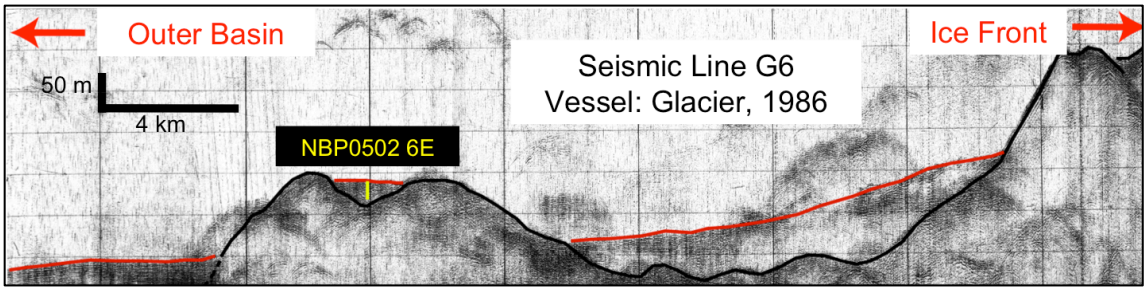

Figure 18. Seismic line G6 of Lapeyrère Bay, with acoustic basement interpreted with black lines, and sediment drapes marked with red lines. Location of core NBP0502 6E is identified in yellow (Fernandez, R., per. com.).

Sediment Core Data

The combination of core analysis methods (grain-size analysis, MSCL data, pebble count, photographs, onboard descriptions, and smear slides) conducted on two cores, NBP0502 6E (Fig. A1-3) and NBP0703 JPC-35 (Fig. A1-2), allowed identification of five sediment facies (Fig. 19). The first is dark olive gray fine-grained sediment, and the second is gray very fine-grained sediment. Though both appear distinctly different, they are each interpreted as open-marine deposits. The third sediment facies is greenish gray medium-grained sediment, and is interpreted as a sequence of turbidites. The fourth facies is very dark greenish gray fine-grained sediment, and is interpreted as glacial outwash fan deposits. The fifth sediment facies is diamicton, interpreted as proximal glacial-marine deposits. Facies and interpretations are described in detail below (Table 1).

Granitoid and basaltic pebbles < 2 mm in diameter were sampled throughout facies 1,3, 4, and 5. Their composition is consistent with the known geology of Anvers Island. Anvers Island is largely composed of Upper Jurassic to Upper Tertiary undifferentiated volcanic rocks, and an Upper Cretaceous to Lower Tertiary Andean Intrusive Suite (Adie, 1969).

Grain-size analysis revealed all facies as dominated by silt-sized particles (particles 4.0 to 63.0 μm in diameter). Diatoms in the modern Gerlache Straight are found to range in diameter from 2-20 μm, and would therefore be recorded as silt-sized in particle-size distributions (Rodriguez et al., 2002). To have only measured the size of terrigenous grains would need to have had diatoms chemically removed prior to analysis. As this was not done, high silt percentages may be taken in part as an indicator of

increased biogenic content, and not a true grain-size measurement. Such grain-size measurements, of both the terrigenous fraction and the biogenic fraction, are typical analysis of modern glacial sediments and allow for comparison to other studies (e.g. Evans et al., 2005; Boyd et al., 2008; Michalchuk et al., 2009; Milliken et al., 2009; Barnard, 2010; Hardin, 2011; Szczucinski and Zajaczkowski, 2010).

Sediment Facies

1. NBP0703 JPC-35 729-761cm

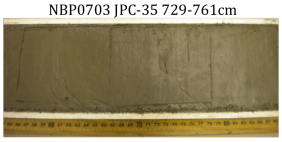

Dark Olive Gray Fine-Grained Sediment
- -mud with occasional fine sand component
- -highly biogenic
- -pebbles dispersed throughout
- -open marine

2. NBP0703 JPC-35 111-147cm

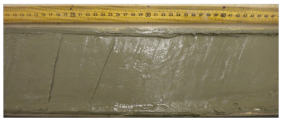

Gray Very Fine-Grained Sediment
- -homogenous mud with no sand component
- -soupy character
- -very highly biogenic with low magnetic susceptibility
- -no pebbles present
- -open marine

3. NBP0703 JPC-35 217-242cm

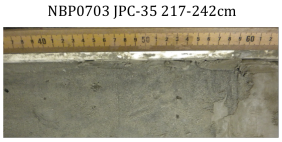

Greenish Gray Medium-Grained Sediment
- -sandy silt packaged by two thick (~5cm) fine sand lenses
- -intermediate biogenic component
- -pebbles frequent
- -series of turbidites

4. NBP0502 6E-1E-1 68-87cm

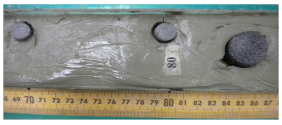

Very Dark Greenish Gray Fine-Grained Sediment
- -homogenous mud with occasional very coarse sand component
- -soupy character
- -low to intermediate shear strength
- -intermediate biogenic component
- -pebbles and Ice Rafted Debris (IRD) frequent
- -glacial outwash fan

5. NBP0502 6E-8E-1 1690-1710cm

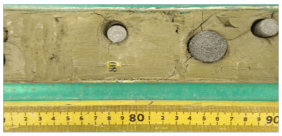

Diamicton
- -sandy mud, with a very coarse sand component
- -intermediate to high shear strength
- -low biogenic component
- -pebbles and Ice Rafted Debris (IRD) frequent
- -proximal glacial marine

Figure 19. Five sediment facies identified in Lapeyrère Bay for cores NBP0703 JPC-35 and NBP0502 6E.

	Sediment Facies 1	**Sediment Facies 2**	**Sediment Facies 3**	**Sediment Facies 4**	**Sediment Facies 5**
Lithology	Dark Olive Gray Fine-Grained Sediment	Gray Very Fine-Grained Sediment	Greenish Gray Medium-Grained Sediment	Very Dark Greenish Gray Fine-Grained Sediment	Diamicton
Interpretation	Open Marine	Open Marine	Series of Turbidites	Glacial Outwash Fan	Proximal Glacial Marine
Average Grain-Size (% sand, silt, clay)	4%, 71%, 25%	0%, 61%, 39%	16%, 65%, 19%	4%, 66%, 30%	9%, 65%, 25%
Biogenic Component	High	High	Intermediate	Intermediate	Low
Bioturbation	Occasional	None	None	None	None
X-ray Facies	Homogenous, Discontinuous Laminations, Continuous Laminations, Bioturbated, Chaotic	Homogenous	Homogenous, Discontinuous Laminations, Chaotic	Homogenous, Discontinuous Laminations, Chaotic, Diamicton	Homogenous, Discontinuous Laminations, Chaotic, Diamicton
Proximal Fjord	Not Present	Not Present	Not Present	NBP0502 6E (0-1500 cm)	NBP0502 6E (1500-2030 cm)
Distal Fjord	NBP0703 JPC35 (0-80 cm and 500-1060 cm)	NBP0703 JPC35 (80-170 cm)	NBP0703 JPC35 (170-500 cm)	Not Present	Not Present

Table 1. Summary of core data and facies interpretations for NBP0703 JPC-35 and NBP0502 6E.

Sediment Facies 1:Dark Olive Gray Fine-grained Sediment

The sediment facies 1 is comprised of highly biogenic mud with an occasional fine sand component. Pebbles are dispersed throughout the facies, with a maximum of 5 pebbles counted in a single horizon, and an average of 1.2 pebbles found in a horizon. Sediment facies 1 is only sampled in the outermost core, NBP0703 JPC-35, and describes the top 80 cm and bottom ~500 cm of the core (Fig. A1-2). Grain-size analysis revealed the facies as a mud with 4% sand, 71% silt, and 25% clay (Fig. 20). The density log through the unit is relatively uniform, averaging 2.3 g/cm^3. Little compaction has taken place in the unit. Magnetic susceptibility data throughout the facies averages a moderate 471.4 SI, indicating a relatively small terrigenous signature. Smear slides support the magnetic susceptibility data, documenting a plethora of non-reworked diatoms (Fig. 21).

The diatoms present are a typical modern western Antarctic Peninsula assemblage and include: *Thalassiosira antarctica, Actinocyclus actinochylus, Cocconeis spp., Fragilariopsis obliquecostata, Fragilariopsis kerguelensis*, with the majority of diatoms being *Chaetoceros* resting spores. The long pennate diatoms, *Fragilariopsis obliquecostata* and *Fragilariopsis kerguelensis*, are indicative of sea ice, which is a common and highly seasonal feature of the western Antarctic Peninsula (Leventer, A., per. com, 2012).

Sediment facies 1 is interpreted as open-marine deposits, as NBP0703 JPC-35 is located in the outer basin far from the modern ice margin (Fig. 10). The top of the core is therefore not recording glacial sediments, but recent open-marine highly biogenic sedimentation (seen in the greenish hue of the facies). If glacial sediments were incorporated in the facies, the particle size distribution would not appear homogenous. Samples would more widely range in grain size due to the various modes of glacial-marine sedimentation.

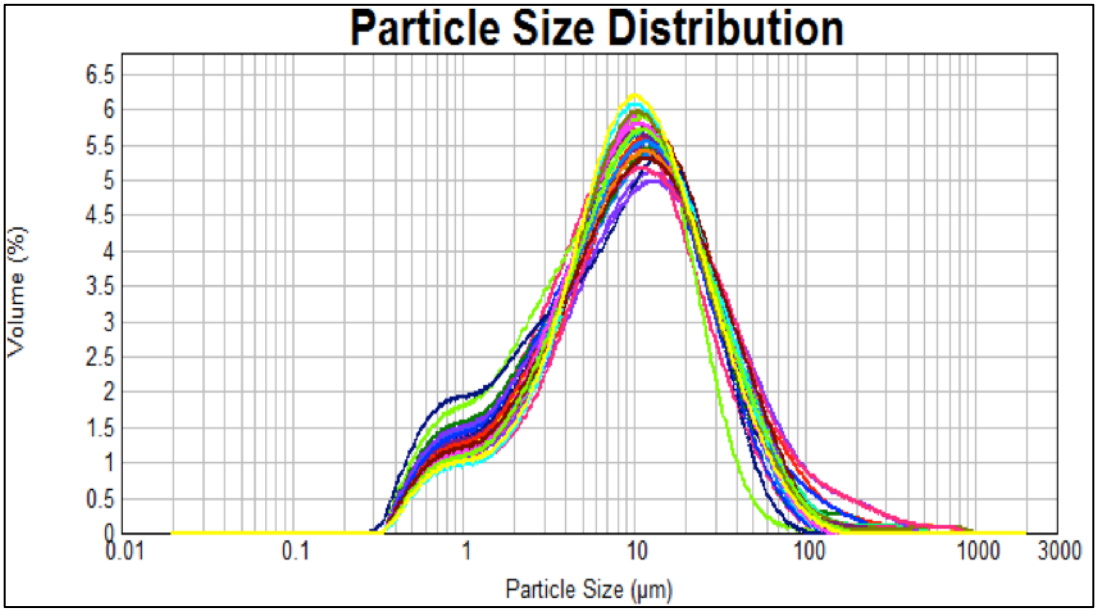

Figure 20. Particle-size distribution of sediment facies 1, interpreted as open-marine sedimentation. Each colored line represents a single 5cc sediment sample taken over a 1 cm horizon, within sediment facies 1, processed using MLPSA. 0.02 to 4.0 µm are clay-sized particles, 4.0 to 63.0 µm are silt-sized particles, and 63.0 to 2000.0 µm are sand-sized particles (Wentworth, 1922).

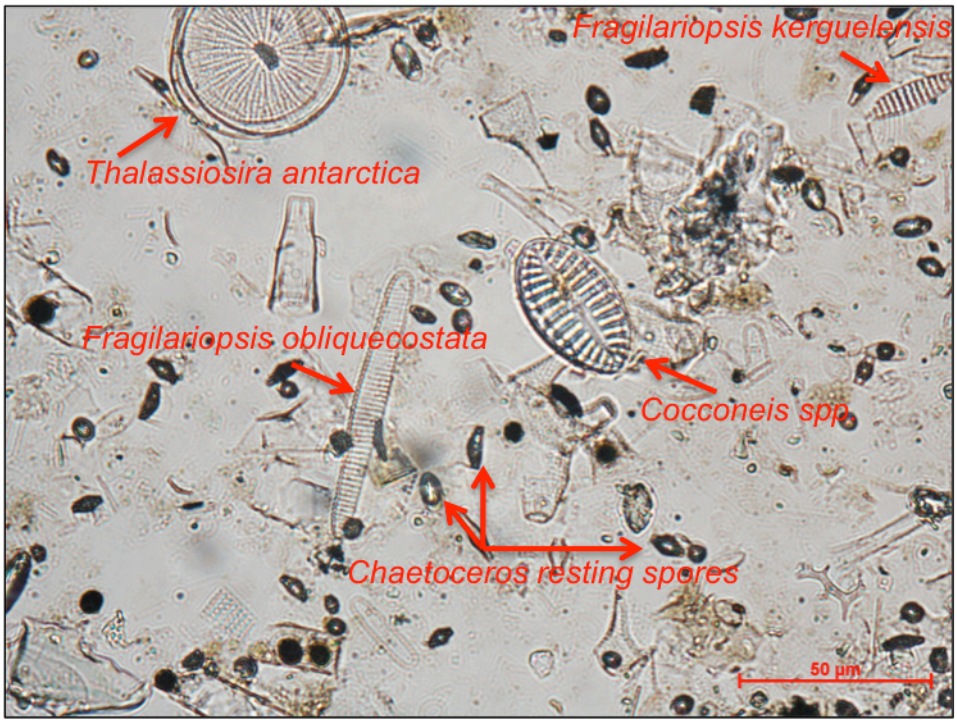

Figure 21. Smear slide of NBP0703 JPC-35 637cm. Diatom abundance supports open-marine sediment interpretation. The red bar indicates a 50 µm scale.

Sediment Facies 2: Gray Very Fine-grained Sediment

Sediment facies 2 is much grayer than sediment facies 1, and is composed of homogenous mud with no sand component. Grain-size analysis described the facies as 61% silt and 39% clay (Fig. 22). No pebbles were found in sediment facies 2. The facies is only identified in NBP0703 JPC-35, and is located between 80 cm and 170 cm of the core (Fig. A1-2). Sediment facies 2 has the lowest average magnetic susceptibility and density measurements found in the core, magnetic susceptibility averaging 282 SI and density averaging 2.1 g/cm^3. Smear slides from the 90 cm section display a significant diatom assemblage. The diatom assemblage and considerably low magnetic susceptibility measurements support sediment facies 2 interpreted as open-marine deposits, because it is highly biogenic despite its grayer character. A likely explanation of the lack of a coarse

sediment fraction is perennial sea ice cover. Fast sea ice during the period would prevent icebergs from traveling into the distal fjord and depositing pebbles and ice rafted debris. Fast sea ice cover would still permit open-marine circulation at depths and the deposition of biogenic sediments.

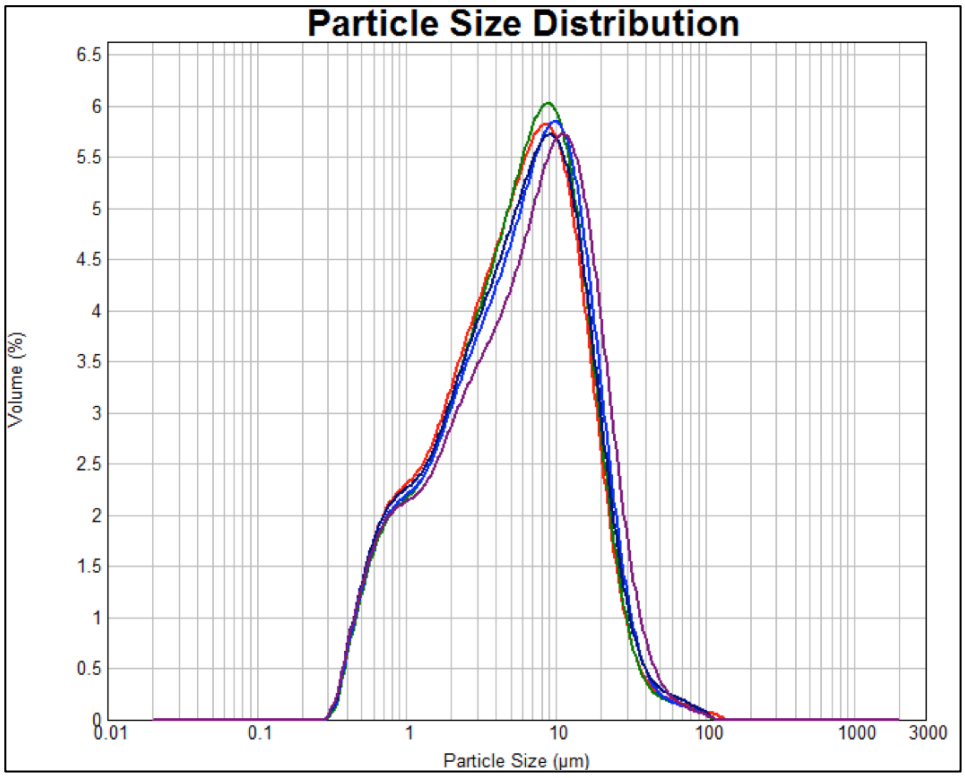

Figure 22. Particle size distribution of sediment facies 2, interpreted as open-marine sedimentation. Each colored line represents a single 5cc sediment sample taken over a 1 cm horizon within sediment facies 2.

Sediment Facies 3:Greenish Gray Medium-grained Sediment

Sediment facies 3 represents a sequence of sandy turbidites. The sequence is found only in NBP0703 JPC-35 between 170 cm and 500 cm (Fig. A1-2). Facies 3 is packaged by two large turbidites, which were preferentially sampled for grain-size analysis. The upper most turbidite is comprised of an average of 49% sand, 45% silt, and 6% clay; whereas the facies as a whole is comprised of an average of 16% sand, 65% silt,

and 19% clay (Fig. 23). The two turbidites have anomalously high magnetic susceptibility measurements; the uppermost (170-220 cm) of 1449.5 SI and the lowermost (480-500 cm) of 853.3 SI, indicating both are primarily terrigenous material. Smear slides also describe a very high terrigenous component. Few diatoms are present, relative to the other NBP0703 JPC-35 facies, whereas a plethora of euhedral grains of micaceous minerals, pyroxenes, and quartz are found (Fig. 24). Density values in the interval are statistically similar to those of sediment facies 1, and average 2.3 g/cm^3. The pebble count for sediment facies 3 average 1.6 pebbles, with a maximum of 6 pebbles found in a single horizon. The terrigenous turbidites were likely deposited as a result of slope failure, either from the northern fjord edge or resulting from erosion of the eastern grounding zone wedge.

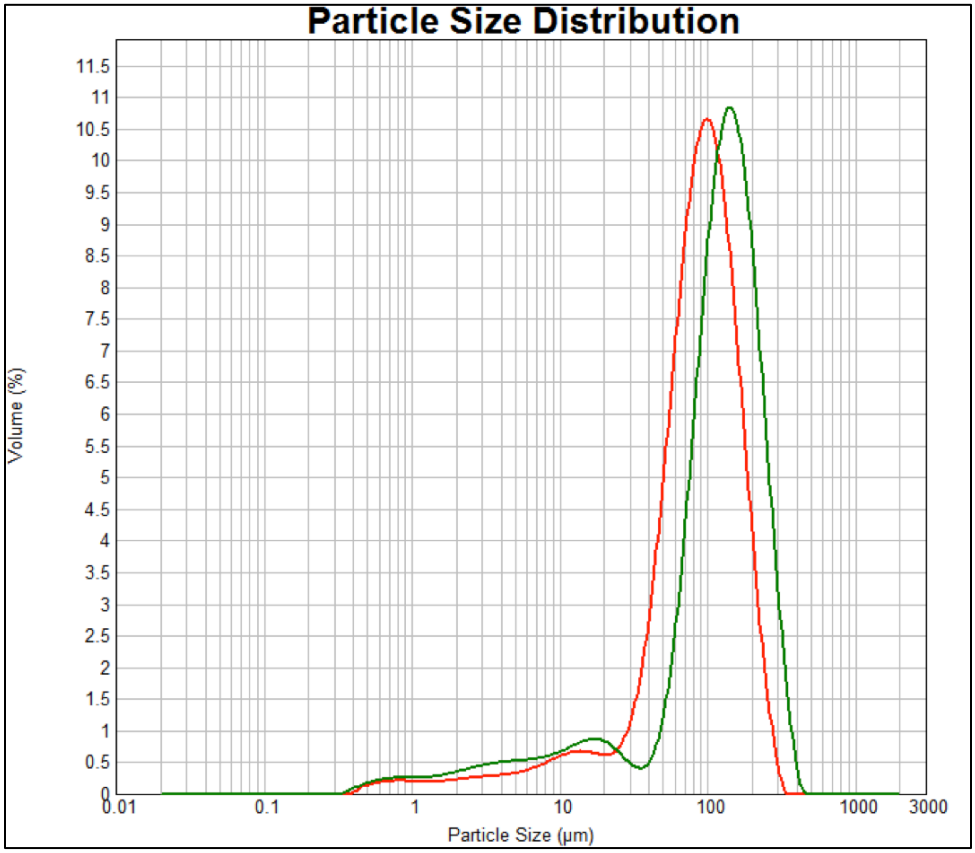

Figure 23. Particle-size distribution of two sandy turbidites packaging sediment facies 3. The green line samples the upper most turbidite (170-220 cm) and the red line samples the lower most turbidite (480-500 cm).

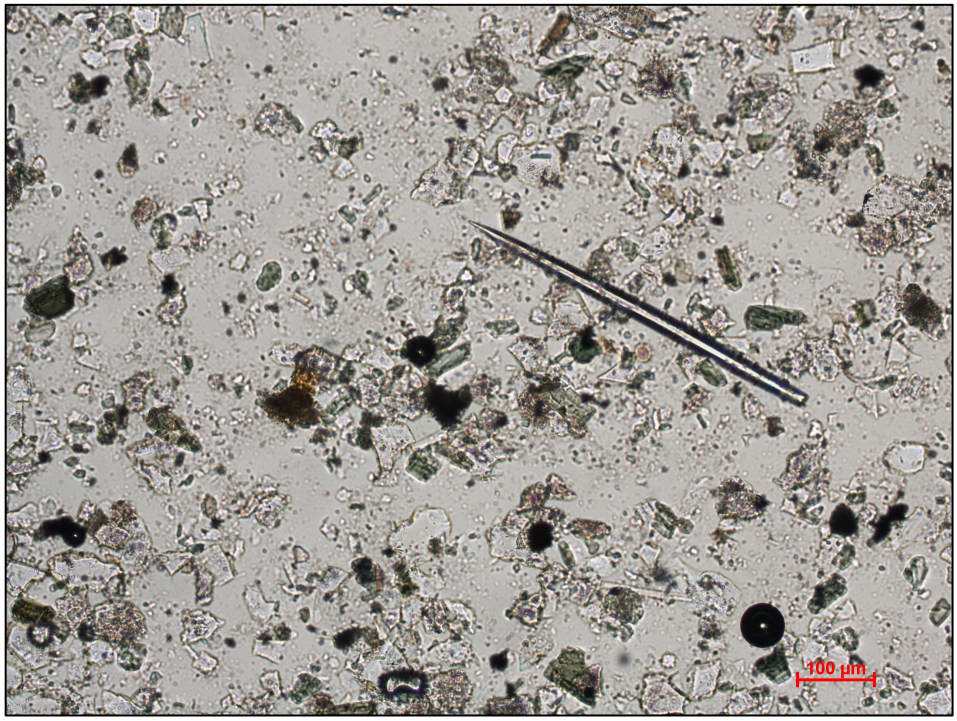

Figure 24. Smear slide of sediment facies 3, NBP0703 JPC-35 190 cm, interpreted as a series of sandy turbidites. Large linear feature is a sponge spicule, but image largely depicts granules and not biogenics. Red bar indicates 100 µm.

Sediment Facies 4:Very Dark Greenish Gray Fine-grained Sediment

Sediment facies 4 is a homogenous mud with an occasional coarse sand component. The coarse component is identified in particle-size analysis as a bimodal curve, even though the facies is dominantly mud, averaging 4% sand, 66% silt, and 30% clay (Fig. 25). Sediment facies 4 is only found in NBP0502 6E, and describes the upper 15 m of the core (Fig. A1-3). The facies shows a coarsening downward trend towards the diamicton facies, and ice-rafted debris (IRD) are found more frequently down-core. MSCL data reveal moderate magnetic susceptibility values, of 198.4 SI, indicating an intermediate biogenic component. Smear slide analysis also identified an intermediate biogenic component in facies 4. Diatoms are present, though some appear fragmented. Pebbles are more frequent in facies 4 than in previously described facies, with an average

of 2.6 pebbles found in horizons every 5 cm down core, and a maximum of 9 pebbles found in a single horizon. Shear strength values were collected for NBP0502 6E using a hand-held Torvane. Sediment facies 4 presents with the lowest shear strength values, averaging ~0.05 kg/cm^2. The facies, especially the upper 8 m, is very soupy. Facies 4 is interpreted as a glacial outwash fan primarily because of its mixed and reworked biogenic and terrigenous signatures. The core is also known to have sampled a glacial outwash fan, as a fan was identified in both multibeam swath bathymetry data and in the G6 air gun seismic line.

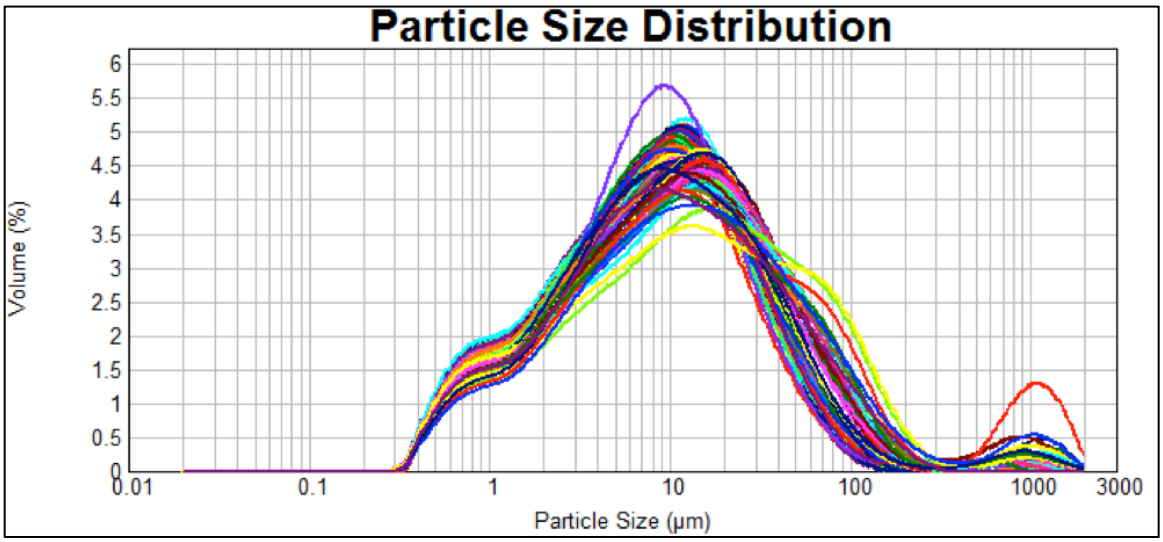

Figure 25. Particle-size distribution of sediment facies 4. Each colored line represents a single 5cc sediment sample taken over a 1 cm horizon, within sediment facies 4. Note the bimodal curve, representing a large homogenous mud component (peaking ~ 10 µm), as well as a smaller coarse sand component (peaking ~1000 µm). The presence of two peaks indicates mixing of glacial terrigenous sediment (~1000 µm peak) and marine highly biogenic sediments (~10 µm peak).

Sediment Facies 5:Diamicton

Sediment facies 5 is a sandy mud containing a similar coarse sand component as sediment facies 4. Facies 5 contains 9% sand, 65% silt, and 26% clay (Fig. 26), and has a lower average and maximum pebble count (1.7 pebbles in a horizon, with a maximum of

8 in a single horizon) than sediment facies 4. Angular ice rafted debris > 5 cm in diameter are common in the facies, and become more frequent and tightly packed down-core (best described by the diamicton x-ray facies). The facies is only identified in NBP0502 6E, specifically the lower 5.3 m of the core (Fig. A1-3). Magnetic susceptibility data reveal a lower biogenic concentration in sediment facies 5, averaging 212.5 SI. Shear strength values are intermediate to high in the facies, all between 0.1 and 0.2 kg/cm^2. Smear slides of the unit display fewer diatoms, and those present appear reworked. The intermediate to high shear strength values, anomalously high IRD packing, and variety of grain sizes specifically indicate glacial-proximal sedimentation. The facies unlikely sampled till, as a small but significant biogenic component is still present (Fig. 27). Below the facies, 13 cm of granite was drilled and sampled. The granite likely indicates a till deposit below sediment facies 5.

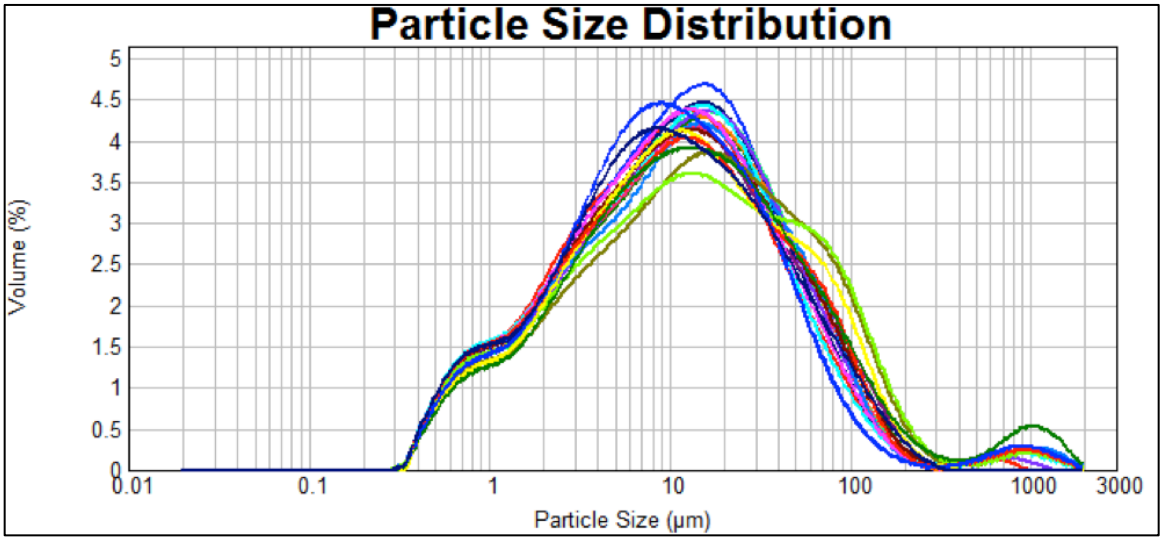

Figure 26. Particle-size distribution describing the diamicton facies. Each colored line represents a single 5cc sediment sample taken over a 1 cm horizon, within sediment facies 5.The distribution is similar to facies 4, and appears bimodal though not as homogenous around either peak.

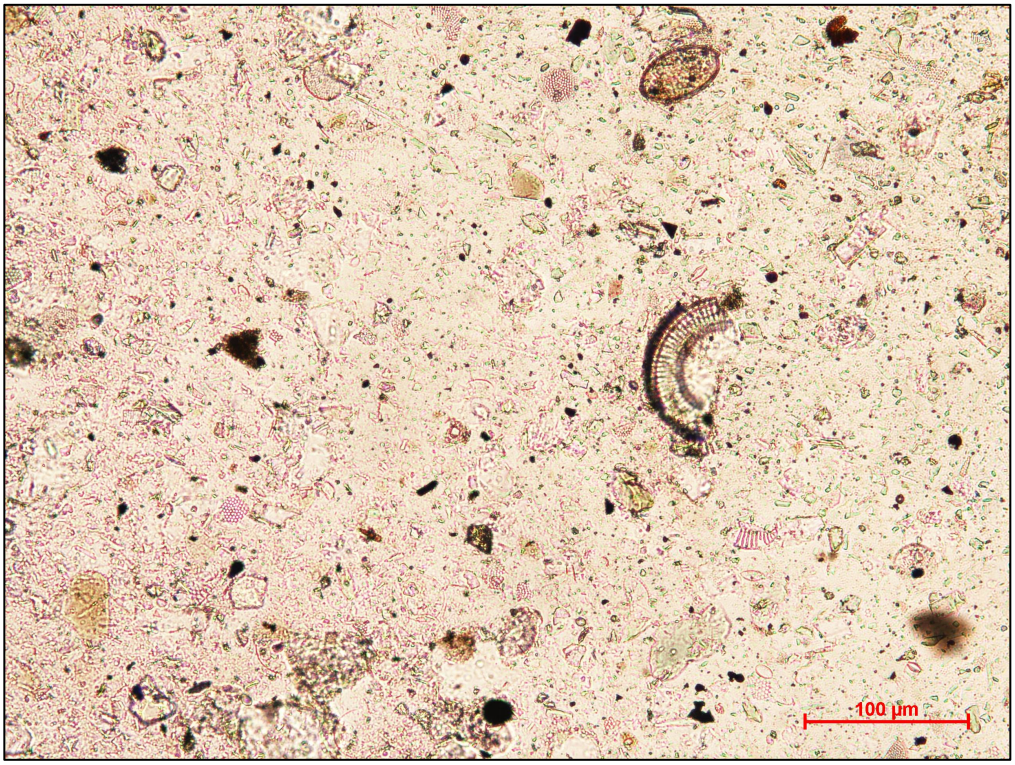

Figure 27. Smear slide of diamicton facies, from NBP0502 1846 cm. The facies has a similar assemblage as facies 4, but appears increasingly reworked. An example is the crescent-shaped diatom in the right of the image. The non-reworked diatom is a full ring shape. The red bar is 100 µm for scale.

X-ray Facies:

X-rays taken of NBP0502 6E and NBP0703 JPC-35 revealed various internal features not seen in photographs or visually described onboard. X-rays express these features through density variations. Using Adobe Photoshop, x-rays were modified, primarily by changing contrast, so that high-density areas appear opaque white and low-density areas, including voids, appear black. Once adjusted, the x-rays were used to count the number of pebbles > 5 mm in horizons selected every 5 cm down core. Five x-ray facies were identified: homogenous, continuously laminated, discontinuously laminated, bioturbated, diamicton, and chaotic (Fig. 28). No bioturbation was found in NBP0502 6E

x-rays, but bioturbation was apparent in three horizons of NBP0703 JPC-35 5-7 m in the form of burrows. These burrows were likely formed by scaphapods, commonly found in Antarctic substrate. A scaphapod shell was collected for carbonate ^{14}C dating in the inner basin NBP0502 6E core. Also noted in x-rays were soft-sediment deformation structures, formed by the deposition of large IRDs (Fig. 29). Through integrating x-ray findings and sediment facies, glacial-marine deposits were interpreted. Bioturbated, continuously laminated, discontinuously laminated, and homogenous x-ray facies were largely found within horizons identified by the dark olive gray fine-grained sediment facies, whereas the diamicton and chaotic x-ray facies were largely found within horizons identified by the diamicton sediment facies.

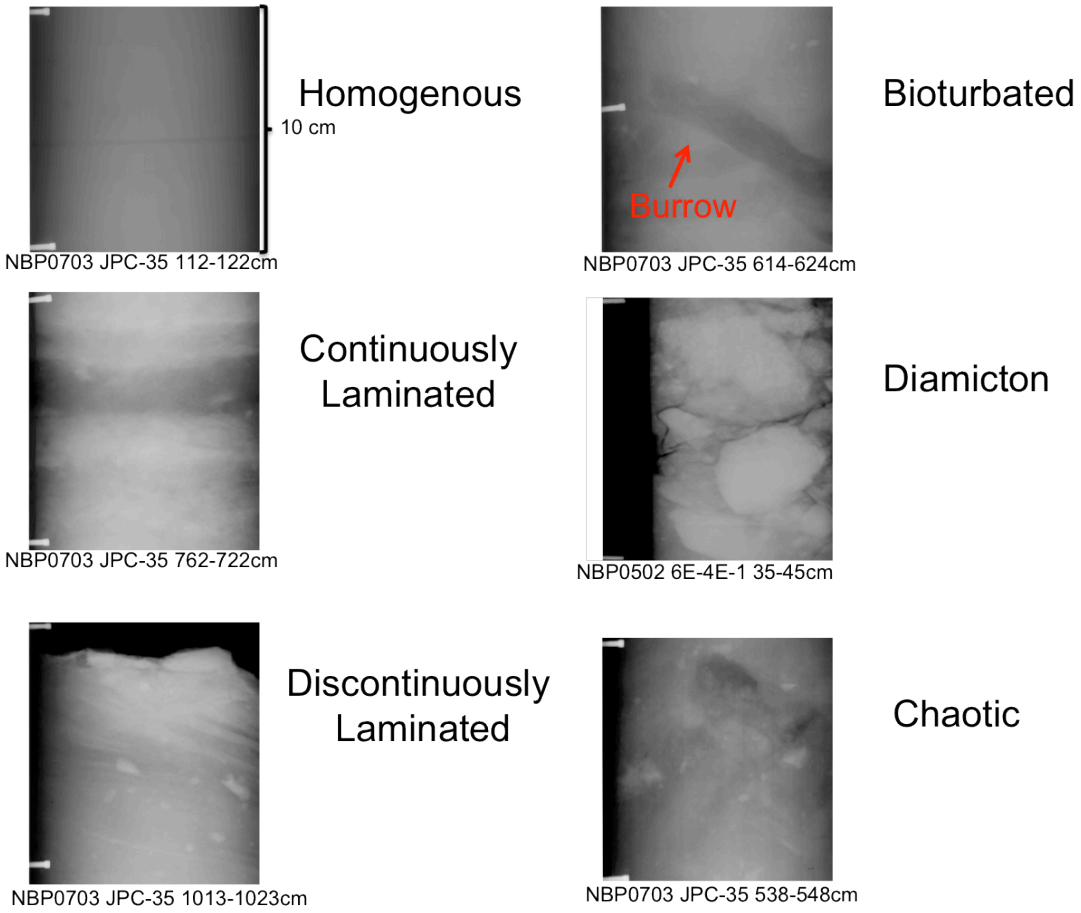

Figure 28. X-ray facies identified in Lapeyrère Bay and found in NBP0502 6E and NBP0703 JPC-35 cores. All images are oriented with the top of the core up and depict 10 cm sections.

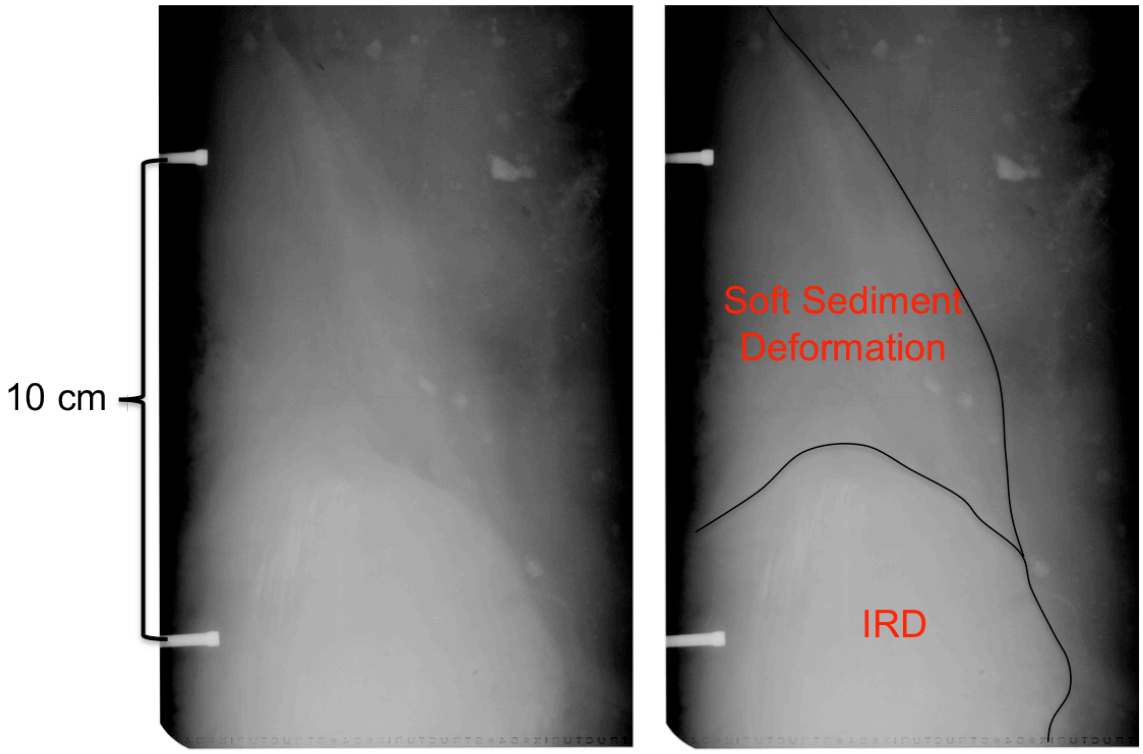

NBP0703 JPC-35 697-712 cm

Figure 29. X-rays depict soft sediment deformation. The left x-ray is uninterpreted, whereas the right x-ray is annotated to show IRD and a dense sediment deformation tail. X-rays orient the top of the core up and the distance between the lines as 10 cm.

Chronology Data

Two cores in Lapeyrere Bay, NBP0502 6E and NBP0703 JPC-35, were analyzed using two ^{14}C dating methods: carbonate ^{14}C dating and ramped pyrolysis ^{14}C dating. NBP0502 6E was sampled the most extensively, with five carbonate dates and ramped pyrolysis ^{14}C dates from six horizons acquired. Four samples were previously carbonate ^{14}C dated in adjacent core NBP0502 KC-6D. Those dates are included in NBP0502 6E age profiles for the most complete chronology. Two carbonate and three ramped pyrolysis dates were collected from the outer fjord core, NBP0703 JPC-35.

Ramped pyrolysis results are not consistent with the previous study by Rosenheim and others (2008) using the method, where ramped pyrolysis was compared to AIOM

dating on cores from the northwestern Weddell Sea (Fig. 13). First, Lapeyrère Bay reaction curves of photometrically resolved CO_2 concentrations during temperature ramp are more complicated than Weddell curves (Fig. 30). Multiple peaks are present within the reaction curves, representing several episodes of increased decomposition rate during pyrolysis. Second, the age spectra from each of these samples was considerably narrower than those in previous work (Rosenheim et al., 2008; Fig. 13), with evidence of some age reversals at higher temperatures (Fig. A2-3). This indicates organic material in Lapeyrère Bay is more homogenous in age than sediment from the previous study. To compare ramped pyrolysis dates to carbonate dates the aliquot with the youngest age was selected as most representative of the true age of the sediment sample. It is assumed, similarly to Rosenheim et al. (2008), that fresh autochthonous organic carbon fixed at the time of sedimentation will decompose at lower temperatures than the older, pre-aged carbon that is admixed into the bulk AIOM.

All calibrated and reservoir-corrected ages for both methods are plausible, ranging from ~700 to ~8500 cal yr BP. They are all in chronological order down-core, with the exception of the second oldest ramped pyrolysis ^{14}C date in NBP0502 6E (6,514 cal yr BP) and the second oldest carbonate ^{14}C date in NBP0703 JPC-35 (1,240 cal yr BP). But, carbonate and ramped pyrolysis ^{14}C dates yield discordant ages. For the proximal core, NBP0502 6E, ramped pyrolysis ages are significantly younger than carbonate ages, and the difference between both methods increases down-core (Fig. 31B). Ramped pyrolysis estimates the maximum age of core as ~4,000 years younger than carbonate ^{14}C ages (Fig. 31C). For the 10.6 m distal gravity core, two carbonate dates are not statistically different and are comparable or younger than ramped pyrolysis dates.

Interpretation down-core is limited by the number of carbonate dates (Fig. 32). Extrapolation of a linear age trend using foraminifera dates is not possible because they are in reverse chronological order down-core. However, the similarity of these ages down-core may be indicative of a source of foraminifera having the same age.

The two dating methods also yield varying sedimentation rates for each core. Ramped pyrolysis estimates a moderate sedimentation rate of ~ 3.3 mm/yr for the outer fjord, whereas carbonate dating estimates a rate of ~ 4.4 mm/yr. For the inner fjord both dating methods estimate lower sedimentation rates, of 2.6 mm/yr by ramped pyrolysis, and 1.8 mm/yr by carbonate ^{14}C dating (Table 2).

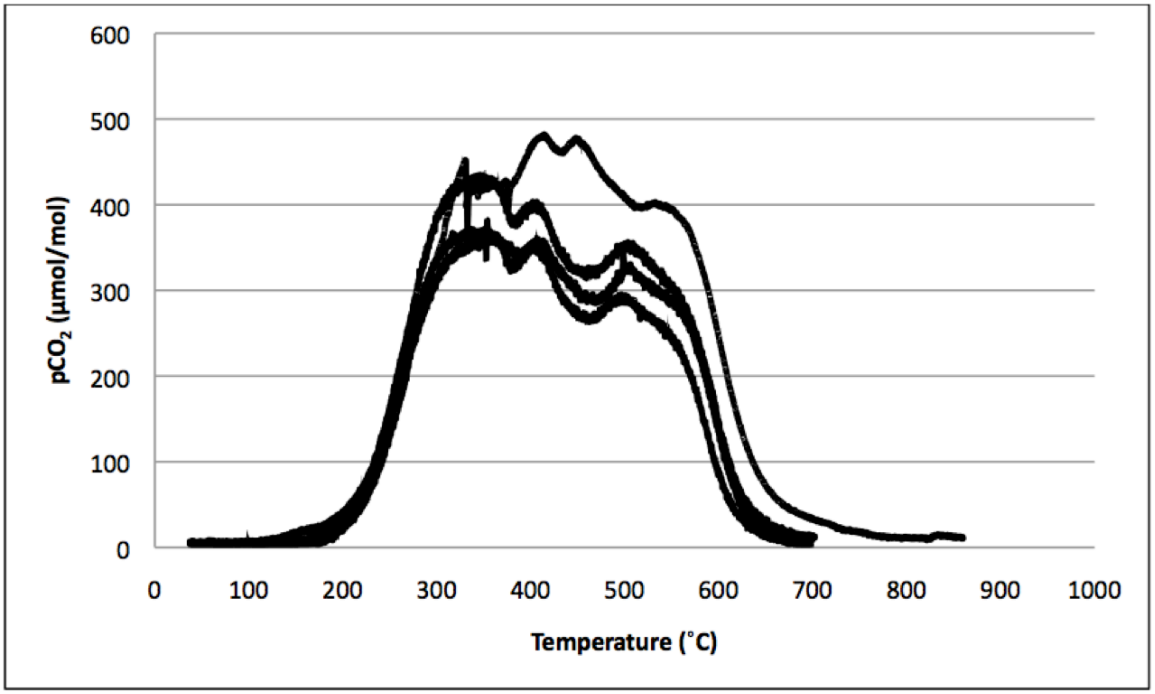

Figure 30. Reaction curves displaying the amount of photometrically measured CO_2 produced at each temperature. The four plotted curves are each from a different combustion run of same sample, NBP0502 6E 245 cm. The curves show very little variation from run to run, but do show multiple peaks, which were not seen in previous studies (Rosenheim et al., 2008).

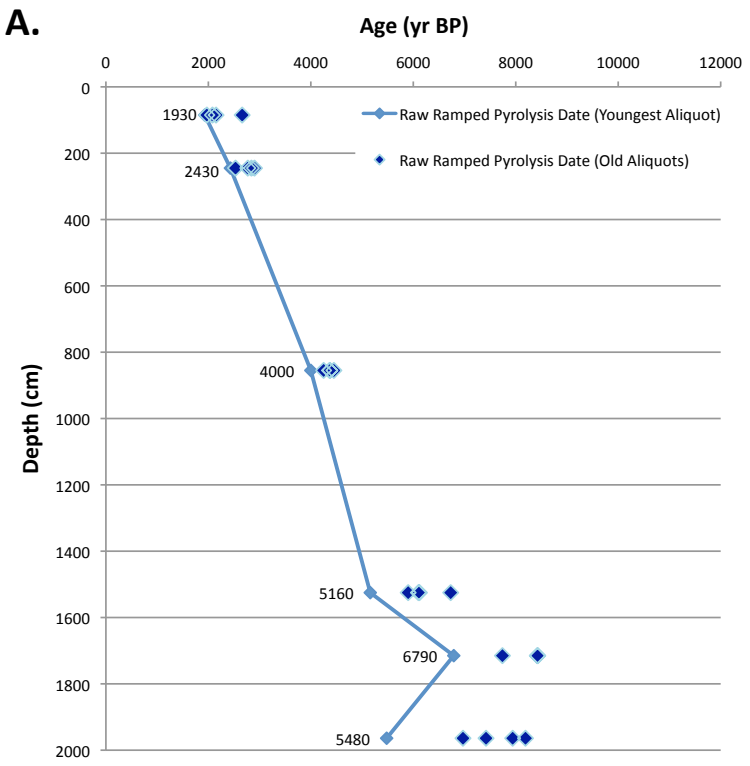
A.
Age (yr BP)
0
2000
4000
6000
8000
10000
12000
Depth (cm)
0
200
400
600
800
1000
1200
1400
1600
1800
2000
1930
2430
4000
5160
6790
5480
Raw Ramped Pyrolysis Date (Youngest Aliquot)
Raw Ramped Pyrolysis Date (Old Aliquots)

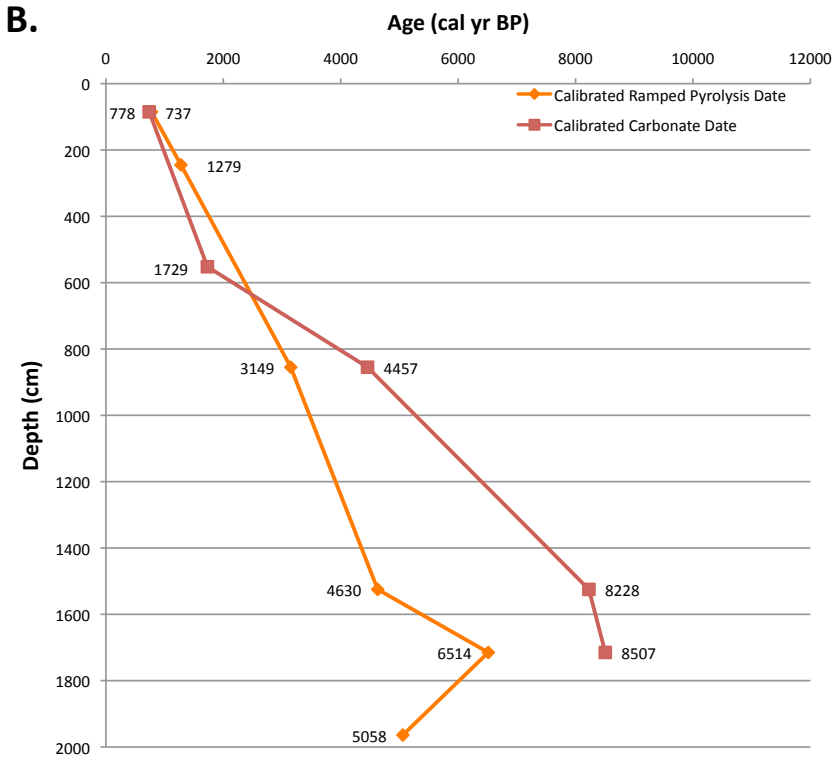
B.
Age (cal yr BP)
0
2000
4000
6000
8000
10000
12000
Depth (cm)
0
200
400
600
800
1000
1200
1400
1600
1800
2000
778
737
1279
1729
3149
4457
4630
8228
6514
8507
5058
Calibrated Ramped Pyrolysis Date
Calibrated Carbonate Date

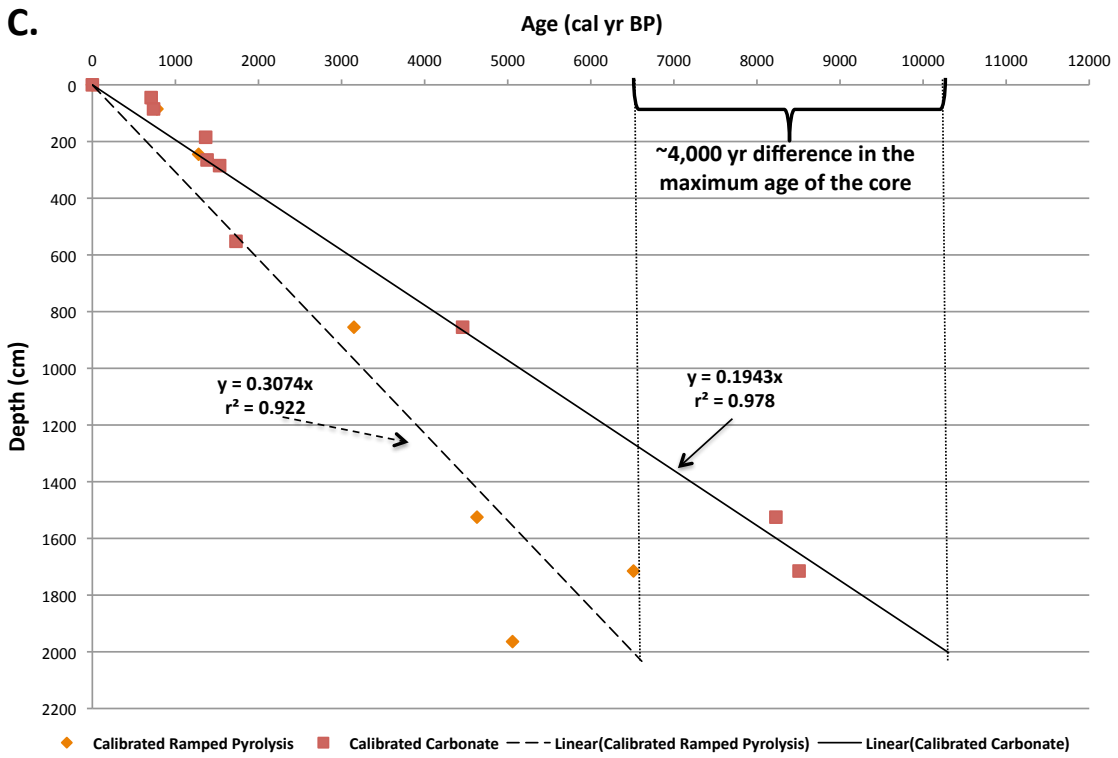

Figure 31. (A) Raw ramped pyrolysis ages plotted down-core for NBP0502 6E. Youngest aliquot ages (true ages) are plotted with older aliquot ages from the same horizons, as the variability in aliquot ages indicates how heterogeneously aged organic carbon is within the sediment. (B) Calibrated and reservoir corrected ramped pyrolysis and carbonate ^{14}C dates plotted down-core for NBP0502 6E. Distance between lines represents the discrepancy between the dating methods. (C) The same data, with the addition of NBP0502 KC-6D carbonate ^{14}C dates. Linear trends are applied to both dating methods and projected to the bottom of the core.

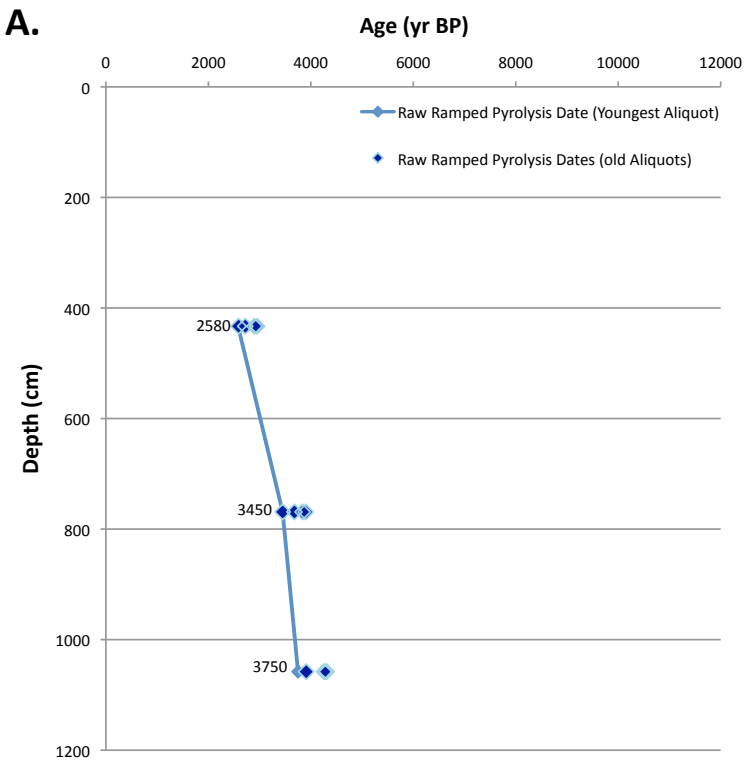
A.
Age (yr BP)
0
2000
4000
6000
8000
10000
12000
Depth (cm)
0
200
400
600
800
1000
1200
Raw Ramped Pyrolysis Date (Youngest Aliquot)
Raw Ramped Pyrolysis Dates (old Aliquots)
2580
3450
3750

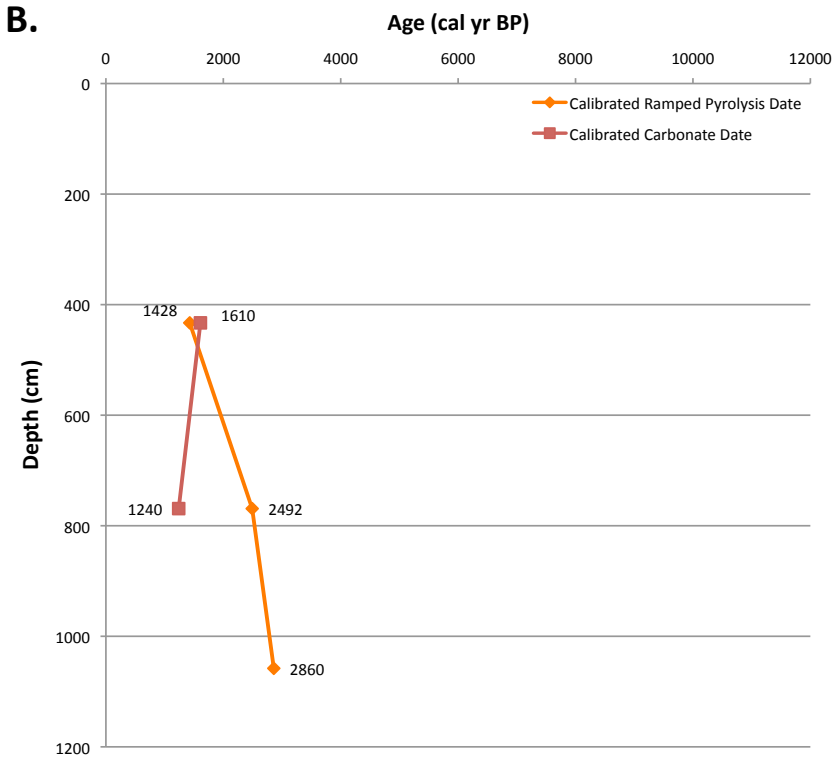
B.
Age (cal yr BP)
0
2000
4000
6000
8000
10000
12000
Depth (cm)
0
200
400
600
800
1000
1200
Calibrated Ramped Pyrolysis Date
Calibrated Carbonate Date
1428
1610
1240
2492
2860

Figure 32. (A) Raw ramped pyrolysis ages plotted down-core for NBP0703 JPC-35. Youngest aliquot ages (true ages) are plotted with older aliquot ages from the same horizons, as the variability in aliquot ages indicates how heterogeneously aged organic carbon is within the sediment. (B) Calibrated and reservoir corrected ramped pyrolysis and carbonate ^{14}C dates plotted down-core for NBP0703 JPC-35. Distance between lines represents the discrepancy between the dating methods.

Dating Method	NBP0502 6E and KC-6D Inner Fjord	NBP0703 JPC-35 Outer Fjord
Calibrated Ramped Pyrolysis ^{14}C	~2.6 mm/yr	~3.3 mm/yr
Calibrated Carbonate ^{14}C	~1.8 mm/yr	~4.4 mm/yr

Table 2. Sedimentation rates, calculated using ramped pyrolysis and carbonate ^{14}C dates, for the inner and outer fjord.

Total Organic Carbon Content

TOC percentages were acquired in the process of prepping samples for ramped pyrolysis dating, but the values are also useful in comparing biogenic components down-core and between two cores (Table 3). Six %TOC values were found for the inner core, NBP0502 6E. The values show no trend down-core, and range from 0.13 to 0.29 %TOC. Three samples were collected for the outer bay core, NBP0703 JPC35, which similarly show no down-core trend. They range from 0.41 to 0.65 %TOC, with all values higher than NBP0502 6E %TOC values (Table 3). This is consistent with the outer fjord location and comparatively higher biogenic component (seen in magnetic susceptibility data) of NBP0703 JPC35 (Fig. A1-2).

Inner Fjord Sample	TOC %
NBP0502 6E1E1 85 cm	0.13
NBP0502 6E2E2 245 cm	0.25
NBP0502 6E4E1 855 cm	0.23
NBP0502 6E7E1 1525 cm	0.23
NBP0502 6E8E1 1715 cm	0.16
NBP0502 6E8E2 1964 cm	0.29

Outer Fjord Sample	TOC %
NBP0703 JPC35-2C 433 cm	0.59
NBP0703 JPC35-3C 769 cm	0.41
NBP0703 JPC35-4B 1058 cm	0.65

Table 3. %TOC values from EA at Tulane University Stable Isotope Laboratory. Values from the inner fjord core (NBP0502 6E) are overall lower than values from the outer fjord core (NBP0703 JPC35).

DISCUSSION

Ramped Pyrolysis

The age differences produced by ramped pyrolysis and carbonate ^{14}C dating call into question the assumption that foraminifera found in a horizon truly represent the age of that horizon. The dates acquired in this study likely describe a degree of reworking of foraminifera prior to deposition in the horizon from which they were sampled. One scenario explaining how inner fjord ramped pyrolysis ages are younger than carbonate ages and how that difference increases down-core, is that Iliad Glacier and unnamed glacier re-advanced in the recent Holocene. As the glaciers then retreated back to the current position old foraminifera were incorporated in glacial sediments. The foraminifera were re-deposited in the glacial outwash fan, through hypopycnal plumes,

along with modern organic matter falling out of suspension. In this case, ramped pyrolysis dates reflect the modern organic carbon and thus the true age of deposition, whereas carbonate dates reflect a mix of inner fjord sediments dated prior and post glacial re-advance.

Another possible scenario is that both Iliad Glacier and the unnamed glacier retreated after the LGM and did not subsequently re-advance. Older foraminifera (~50-3,500 cal yr BP older) could be deposited with young organic matter through constant re-suspension in the water column and mixing by turbidity flows from the steep northern fjord edge. Both scenarios supply younger organic matter, dated by ramped pyrolysis, and older foraminifera, dated by carbonate ^{14}C, in Lapeyrère Bay and are in agreement with sediment core descriptions.

Sources of Uncertainty

Though the laboratory errors from AMS analysis are extremely small, multiple other sources of uncertainty affect chronology results in this study, including the ^{14}C reservoir correction, sampling methods, and ramped pyrolysis producing maximum possible ages.

A ^{14}C reservoir correction is necessary when dating material developed in a marine setting, as ocean waters contain old carbon. In the Antarctic, this correction is typically much greater than in equatorial settings. However, there are various methods of constraining the reservoir. The reservoir correction applied in this study, 1100 ^{14}C yr BP, was found by Milliken et al. (2009) by dating sediment found at the core-water interface, the sediment assumed most modern and deposited at 0 cal yr BP. The sediment dated 1160 $\pm$ 40 ^{14}C yr BP; therefore a minimum reservoir correction of 1100 ^{14}C yr BP may be

applied down-core. This study was unable to apply carbonate ^{14}C dating to the sediment-water interface of NBP0502 6E and NBP0703 JPC-35, as the top of each core lacked enough calcareous material for AMS processing.

Additionally, a reservoir correction may be constrained by dating other modern materials; including dating dissolved inorganic carbon (DIC) in the water column and by dating corals. The age of DIC in western AP waters ranges from 1000 to 1130 ^{14}C yr BP, comparable to the top-sediment reservoir (Milliken et al., 2009). This is of course a measure only of the modern reservoir of old carbon, but the fact that it is relatively consistent through different water masses suggests that it may not have changed much over time. Hall et al. (2010) assessed the ^{14}C reservoir of the Southern Ocean by dating solitary corals found in the McMurdo Ice Shelf of the Ross Sea. By pairing U/Th and ^{14}C analysis (based on the ^{14}C signature of mid 20th century bomb testing) of the corals, they found a reservoir age of 1144 $\pm$ 120 years. U/Th data revealed the corals range in age from modern to ~6000 yr BP, yet all corals yielded a reservoir age around 1144 years. Therefore, according to Hall and others (2010), the reservoir age has been relatively consistent throughout the past 6000 years with only minor perturbations, irresolvable by current the data set.

Sampling also adds a degree of geologic error to the chronology of Lapeyrère Bay. Varying amounts of sediment were used to obtain dates, between 5cc and 20cc samples. Each of these sediment samples represents a minimum of a 1 cm, and up to 10 cm, interval of the core, not a discrete horizon, which affects the age profile for both ramped pyrolysis and carbonate ^{14}C dating. Specifically for carbonate ^{14}C dating, many foraminifera (~100) are collected after sieving a sediment sample. Each foraminifera test

likely has a different age, but as all foraminifera of a sample are combusted together in AMS processing, the carbonate ^{14}C date of the sample is an average of the ages of all foraminifera tests collected for that sample.

Finally, the true ages yielded by ramped pyrolysis are best described as maximum possible ages. Each aliquot contains CO_2 produced by a mixture of organic carbon. The true age of the sample is taken as the aliquot of the youngest age, as it is less likely that the sample was contaminated by young carbon than old carbon. However, the youngest aliquot still represents a mixture of OC of different ages. If the aliquot was taken over a smaller temperature range for instance, the sample would likely date younger, as it would contain a larger portion of diagenetically unstable carbon and a smaller portion of older reworked carbon. The error of dating organic carbon may therefore be described by the variability in aliquot ages of a sample, as they represent how mixed carbon of different ages is within the horizon.

Glacial Reconstruction

During the LGM ice extended to the AP continental shelf; it then receded into the middle and inner shelf ~14,000 cal yr BP (Heroy and Anderson, 2007; Fig. 33A). In the first scenario, glaciers subsequently retreated between ~14,000 cal yr BP and ~8,500 cal yr BP, the maximum carbonate ^{14}C age (Fig. 33B). This retreat allowed for foraminifera deposition in the glacial-proximal setting through ocean circulation (NBP0502 6E). Unnamed glacier and Iliad Glacier then re-advanced between ~8,500 cal yr BP and ~5,000 cal yr BP, the difference in maximum ages from carbonate ^{14}C and ramped pyrolysis ^{14}C ages in NBP0502 6E (Fig. 33C). The maximum extent of re-advance formed the distal-most grounding zone wedge, and excavated older foraminifera to be

incorporated in glacial sediments. Then, between ~5,000 cal yr BP and present, glaciers stepped back into the fjord, depositing the two proximal grounding zone wedges (Fig. 33D). As Iliad Glacier retreated, the older reworked foraminifera deposited in the glacial outwash fan, through meltwater plumes, along with modern organic matter falling out of suspension. Core descriptions of NBP0502 6E and NBP0703 JPC-35 conform to this scenario as well as the second scenario. However, foraminifera identified in the Lapeyrère Bay proximal core, NBP0502 6E, were largely intact (Fig. 11). Foraminifera reworked through glacial re-advance would be broken and fractured. This supports the second scenario as the more likely glacial reconstruction of Lapeyrère Bay.

The second scenario similarly describes a degree of foraminifera reworking, but without a glacial re-advance between ~8,500 and ~5,000 cal yr BP. In this scenario, Iliad and unnamed glaciers retreated into Lapeyrère Bay, to their current locations, between ~14,000 and ~8,500 cal yr BP (Fig. 33A,C-D). This retreat began highly biogenic open-marine sedimentation in the outer fjord (NBP0703 JPC-35). In retreat the glaciers paused twice, first depositing the distal and then approximately contemporaneously the two proximal grounding zone wedges. A high average shear strength, variable grain-size, and high IRD compaction in the diamicton x-ray facies document the proximal glacial-marine setting of NBP0502 6E during the retreat. Between ~8,500 cal yr BP and present, foraminifera have been continually re-suspended and mixed by turbidite flows prior to deposition with modern organic matter in the glacial outwash fan deposit (Fig. 33E). During this time the inner fjord core, NBP0502 6E, records the deposition of a glacial outwash fan through a highly reworked IRD and pebble-rich diamicton x-ray facies, increased average grain sizes, and a low biogenic component. This is supported by the

lack of bioturbation identified in x-rays and broken diatom assemblages described in smear slides.

Presently, Iliad Glacier is stabilized on a basement high, as seen in the seismic data. The stance is typical of fjord-confined glacial retreat patterns (Fernandez et al., 2011; Fig. 33E). Between ~5,000 cal yr BP and present the distal core, NBP0703 JPC35, records open-marine sedimentation through lower average grain sizes, abundant and diverse diatom assemblages, relatively high TOC values, and bioturbation identified in x-ray facies. The open-marine deposits are punctuated by a series of turbidites, likely from a grounding zone wedge destabilization between ~1,500 cal yr BP and present.

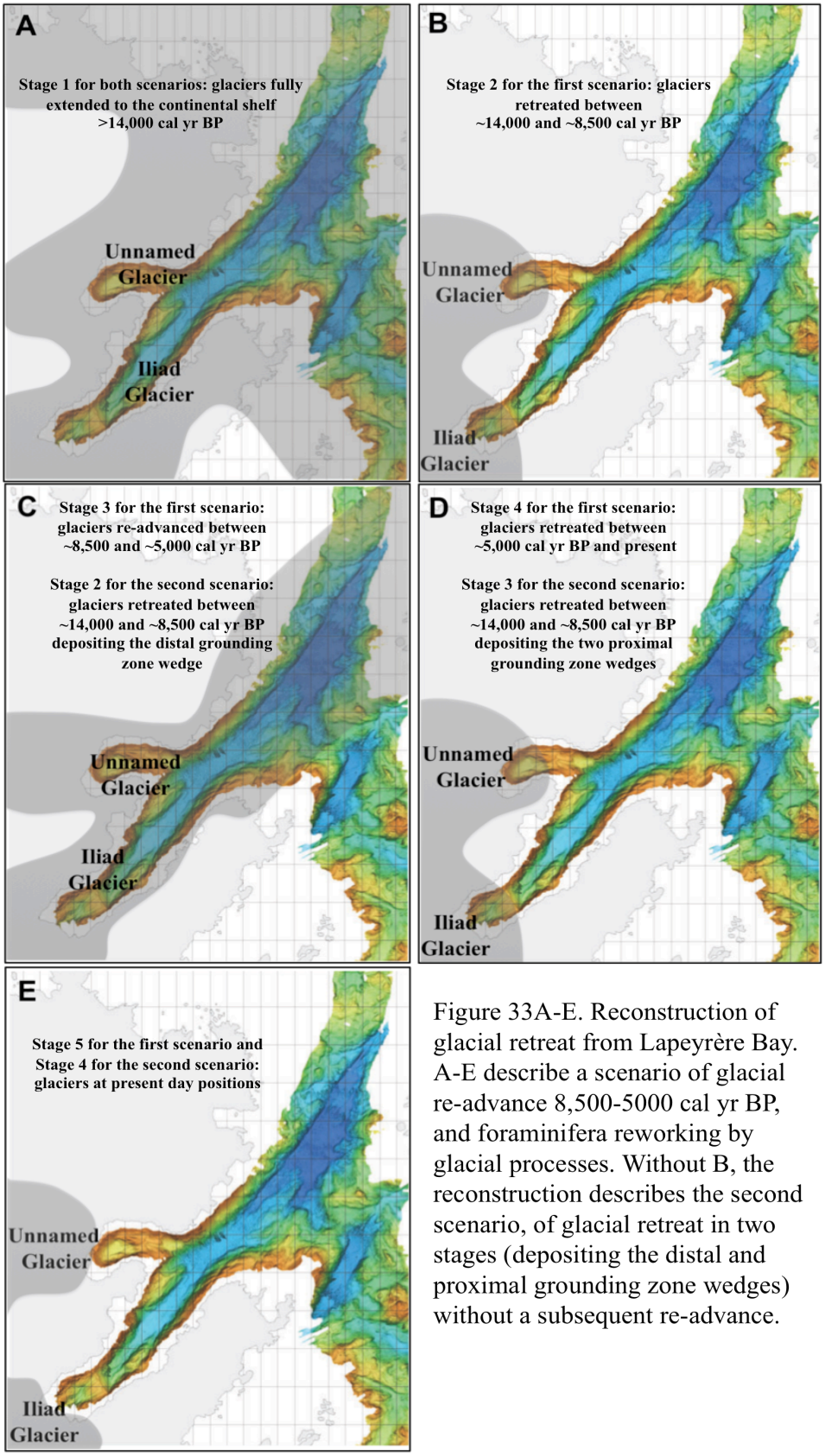

Figure 33A-E. Reconstruction of glacial retreat from Lapeyrère Bay. A-E describe a scenario of glacial re-advance 8,500-5000 cal yr BP, and foraminifera reworking by glacial processes. Without B, the reconstruction describes the second scenario, of glacial retreat in two stages (depositing the distal and proximal grounding zone wedges) without a subsequent re-advance.

The timing of glacial retreat from Lapeyrère Bay (in both scenarios) is consistent with findings from a study conducted by Hall and others (2010) on the Maar Piedmont of southern Anvers Island. By radiocarbon dating shells and moss-rich peat samples from land, they concluded ice was at or further receded from its current position 700-970 cal yr BP. Shelled organisms could not have lived and peat could not have deposited if the area was ice covered. This thesis supports the theory as foraminifera, indicative of ocean circulation, were deposited in Lapeyrère Bay ~8,500 cal yr BP. Retreat from northern Anvers Island followed by the southern Maar Piedmont of Anvers Island agrees with the trend found by Heroy and Anderson (2007) of deglaciation beginning in the northern AP and progressing southward. Deglaciation of northern Anvers Island ~8,500 cal yr BP, is also consistent with other AP studies describing deglaciation of most presently ice-free areas occurring between ~10,000 and 6,500 cal yr BP, followed by several periods of possible glacial re-advance (e.g. Ingolfsson, 1998; Milliken et al., 2009).

A study by Hardin (2011) of Beascochea Bay, ~130 km to the south of Lapeyrère Bay, applied ^{210}PB, ^{137}Cs, and ^{14}C dating techniques to 10 marine sediment cores and found glaciers fully retreated from the bay between ~1,800 and ~1,600 cal yr BP, and subsequently re-advanced. Deglaciation to present day conditions occurred ~170 cal yr BP in Beascochea Bay. This retreat is considerably more recent than findings for Lapeyrère Bay, and is likely explained by geographic variance. Lapeyrère Bay is situated on the northern outer rim of Anvers Island, vulnerable to high winds and cyclones off the Bellingshausen Sea, and warmer open ocean circulation. Conversely, Beascochea Bay is farther south, and buffered from open ocean weather systems, which would aid in

deglaciation, by the series of islands lining the western AP including Anvers Island to the north and Renaud Island to the south.

Late Holocene Climate

Sediment core, geochemical, and multibeam data from Lapeyrère Bay do not display late Holocene climate fluctuations, including the Little Ice Age and Mid-Holocene Warm Period (Fig. 4). The two cores examined in this study, one largely sampling a glacial outwash fan deposit, may not be a high enough resolution survey to identify recent century-scale climate events.

Sedimentation Rates

Sedimentation rates in Lapeyrère Bay were found to be higher in the distal fjord than in the proximal fjord by both dating methods. The distal fjord average sedimentation rate is between ~3.3-4.4 mm/yr, a relatively high sedimentation rate, and the proximal fjord average sedimentation rate is between ~1.8-2.6 mm/yr, a relatively moderate sedimentation rate. These values are unexpected, as typically sedimentation rates increase closer to the ice front. For instance Flandres Bay, ~60 m southwest of Lapeyrère Bay, has a high sedimentation rate of ~8.3 mm/yr near the ice margin, almost four times the inner fjord sedimentation rate of Lapeyrère Bay. Outer Flandres average sedimentation rate is ~4.2 mm/yr, comparable to what was found in distal Lapeyrère Bay. The higher average sedimentation rate in the outer fjord compared to the inner fjord of Lapeyrère Bay may be a result of high productivity in the water column, and consequently rapid deposition of diatoms. This is documented by the high silt content in NBP0703 JPC35 particle size distributions, as diatoms are silt-sized, and by the plethora of *Chaetoceros* resting spores

identified in smear slides. *Chaetoceros* resting spores are indicative if high surface water productivity (Leventer, A., per. com, 2012).

CONCLUSIONS

Lapeyrère Bay is a fjord, as multibeam swath bathymetry surveys have revealed 30º steeply sloping walls. Multibeam also revealed two grounding zone wedges, indicative of two pauses in glacial flow. A glacial outwash fan is located on the northern wall of the proximal fjord, supplied by hypopycnal sediment-laden plumes. Seismic data from the bay describes two basement highs in the proximal fjord, one at the modern ice front and one beneath the glacial outwash fan deposit. Between the highs is a ~40 m thick draping of sediment. Two cores, one from the proximal fjord and one from the distal fjord, are described by five sediment facies, which are interpreted as open-marine, turbidite, glacial outwash fan, and proximal glacial-marine deposits. Similarly, cores were described using six x-ray facies. The density contrast between dense material and voids allowed bioturbation and laminations to be observed. TOC values were used as a proxy for organic content in the proximal and distal fjord. TOC values do not show a down-core trend, but outer fjord values are overall higher than inner fjord values.

To put facies interpretations in the context of glacial retreat, and to calculate sedimentation rates, two methods of ^{14}C dating were applied: carbonate ^{14}C dating of foraminifera, and ramped pyrolysis ^{14}C dating of individual fractions of organic matter. Ramped pyrolysis results differ from previous studies. Age spectra produced by each sediment sample are narrower than expected and not always increasing with temperature. This indicates sediment in Lapeyrère Bay is more homogenous in age than sediment from the previous Weddell Sea study. Applying the date of the youngest aliquot, in the

proximal core ramped pyrolysis ages are significantly younger than carbonate ages, and the difference between both methods increases down-core. In the distal gravity core, two carbonate dates are comparable to or younger than ramped pyrolysis dates. The two dating methods also yield varying sedimentation rates for each core, though both methods yield lower rates for the inner fjord than the outer fjord.

To explain the differences in dating methods, two scenarios of glacial retreat are described in which old foraminifera are reworked and deposited with modern organic matter. The first scenario is a full deglaciation of Lapeyrère Bay between ~14,000-8,500 cal yr BP followed by a re-advance of Iliad and unnamed glaciers ~8,500-5,000 cal yr BP. From ~5,000 cal yr BP to present glaciers again retreated to their modern position. During this retreat foraminifera, reworked by the glacial fluctuation, were deposited in the glacial outwash fan with modern organic matter falling out of suspension.

The second scenario for glacial retreat from Lapeyrère Bay is a full deglaciation between ~14,000 and ~8,500 cal yr BP without subsequent re-advance. In this scenario foraminifera are reworked through turbidite flows and constant re-suspension prior to deposition in the glacial outwash fan. Deglaciation ~8,500 cal yr BP is consistent with findings from southern Anvers Island, and follows the trend of progressive deglaciation from the northern to southern AP. This is a more likely scenario, as foraminifera found in the proximal fjord are not fractured or broken by glacial reworking, as one would expect in scenario 1.

The difference in dates yielded by ramped pyrolysis and carbonate ^{14}C methods may indicate the glacial retreat history of other Antarctic bays and fjords are more complex than previously recognized. Most sediment cores from the region are dated

using solely carbonate ^{14}C, and the dates are assumed to represent accurately the horizon sampled if they in chronological order down-core. In this study most carbonate ^{14}C ages were largely in chronological order down-core, yet they appear to represent extensive foraminifera reworking prior to deposition, as seen by ramped pyrolysis. Placing carbonate dates in this context may dramatically change the interpretation of glacial retreat from Antarctic bays. Applying two methods of dating in Lapeyrère Bay resulted in sediment cores interpreted as ~4000 cal yr BP younger, possibly documenting a glacial re-advance. The "gold standard" of dating Antarctic sediment cores, carbonate ^{14}C dating, may not be as reliable as previously thought.

REFERENCES CITED

Adie, R.J., 1969. Geologic map of Antarctica: Sheet 1, Northern Antarctic Peninsula. American Geographical Society. Scale 1:1,000,000.

Anderson, J.B., Shipp, S.S., Lowe, A.L., Wellner, J.S., Mosola, A.B., 2002. The Antarctic Ice Sheet during the Last Glacial Maximum and its subsequent retreat history: A review. Quaternary Science Reviews, Vol. 21, p. 49-70.

Ashley, G.M., and Smith, N.D., 2000. Marine sedimentation at a calving glacier margin. Geological Society of America Bulletin, Vol. 112, p. 657-667.

Barnard, A., 2010. Onset of a small but significant regional climate change documented in high-resolution late Holocene sediment cores from the maritime western Antarctic Peninsula (Unpublished M.S. Thesis, University of Houston).

Bentley, M.J., Hodgson, D.A., Smith, J.A., O Cofaigh, C., Domack, E.W., Larter, R.D., Roberts, S.J., Brachfeld, S., Leventer, A., Hjort, C., Hillenbrand, C-D., Evans, J., 2009. Mechanisms of Holocene paleoenvironmental change in the Antarctic Peninsula region. Holocene, Vol. 19, p. 51-69, doi:10.1177/0959683608096603.

Bjorck, S., Hjort, C., Ingolfsson, O., Skog, G., 1991. Radiocarbon dates from the Antarctic Peninsula-problems and potential, *in* Lowe, J.J., ed., Radiocarbon dating: recent applications and future potential. Quaternary Proceedings, Cambridge Quaternary Research Association, Vol. 1, p. 55-65.

Boyd, B.L., Anderson, J.B., Wellner, J.S., Fernandez, R.A., 2008. The sedimentary

record of glacial retreat, Marinelli Fjord, Patagonia: Regional correlations and climate ties. Marine Geology, Vol. 255, p. 165-178.

Cook, A.J., Fox, A.J., Vaughan, D.G., Ferrigno, J.G., 2005. Retreating glacier fronts on the Antarctic Peninsula over the past half-century. Science, Vol. 308, p. 541-544.

Domack, E.W., and Ishman, S., 1993. Oceanographic and physiographic controls on modern sedimentation within Antarctic fjords. Geologcal Society of America Bulletin, Vol. 105, p. 1175-1189.

Domack, E.W., Jull, A.J.T., Anderson, J.B., Linick, T.W., Williams, C.R., 1989. Application of tandem accelerator mass-spectrometer dating to Pleistocene-Holocene sediments of the East Antarctic continental shelf. Quaternary Research, Vol. 31, p. 277-287.

Domack, E.W., Leventer, A., Dunbar, R., Taylor, F., Brachfeld, S., Sjunneskog, C., 2001. Chronology of the Palmer Deep site, Antarctic Peninsula; A Holocene paleoenvironmental reference for the circum-Antarctic. Holocene, Vol. 11, p. 1-9.

Evans, J., Pudsey, C.J., OCofaigh, C., Morris, P., Domack, E., 2005. Late Quaternary glacial history, flow dynamics and sedimentation along the eastern margin of the Antarctic Peninsula. Quaternary Science Reviews, Vol. 24, p. 741-774.

Fernandez, R.A., Anderson, J.B., Wellner, J.S., Hallet, B., 2011. Timescale dependence of glacial erosion rates, a case study of Marinelli Glacier, Cordillera Darwin, southern Patagonia. Journal of Geophysical Research, doi: 10.1029/2010JF001685.

Fernandez, R.A., personal written communication, January 2012 (Rice University).

Griffith, T.W., and J.B., Anderson, 1989. Climatic control of sedimentation in bays and fjords of the northern Antarctic Peninsula. Marine Geology, Vol. 85, p. 181-204.

Gustavson, T.C., and Boothroyd, J.C., 1987. A depositional model for outwash, sediment sources, and hydrologic characteristics, Malaspina Glacier, Alaska: A modern analong of the southeastern margin of the Laurentide Ice Sheet. Geological Society of America Bulletin, Vol. 99, p. 187-200.

Hall, B.L., Koffman, T., Denton, G.H., 2010. Reduced ice extent on the western Antarctic Peninsula at 700-970 cal. yr B.P. Geology, Vol. 38, p. 635-638.

Hall, B.L., Henderson, G.M., Baroni, C., Kellogg, T.B., 2010. Constant Holocene Southern-Ocean ^{14}C reservoir ages and ice-flow rates. Earth and Planetary Science Letters, Vol. 296, p. 115-123.

Hardin, L., 2011. High-resolution Holocene glacial-marine sediment facies analysis of Beascochea Bay, western Antarctic Peninsula, Antarctica (Unpublished M.S. Thesis, University of Houston).

Heroy, D.C., and Anderson, J.B., 2005. Ice-sheet extent of the Antarctic Peninsula region during the Last Glacial Maximum (LGM): Insights from glacial geomorphology. Geological Society of America Bulletin, Vol. 117, p. 1497-1512.

Heroy, D.C., and Anderson, J.B., 2007. Radiocarbon constraints on Antarctic Peninsula Ice Sheet retreat following the Last Glacial Maximum (LGM). Quaternary Science Reviews, Vol. 26, p. 3286-3297.

Ingolfsson, O., Hjort, C., Berkman, P., Bjork, S., Colhoun, C., Goodwin, I.D., Hall, B., Hirakawa, K., Melles, M., Moller, P., Prentice, M., 1998. Antarctic glacial history since the Last Glacial Maximum: An overview of the record on land. Antarctic Science, Vol. 10, p. 326-344.

Ishman, S., personal oral communication, March 2012 (Southern Illinois University).

Joughin, I., and Alley, R.B., 2011. Stability of the West Antarctic ice sheet in a warming world. Nature Geoscience, Vol. 4, p. 506-513.

Kaiser, J., Lamy, F., Hebbeln, D., 2005. A 70-kyr sea surface temperature record off southern Chile (Ocean Drilling Program Site 1233). Paleoceanography, Vol. 20, p. 4009, doi: 10.1029/2005PA001146.

Khim, B.K., Shim, J., Yoon, H.I., Kang, Y.C., Jang, Y.H., 2007. Lithologic and biogenic particle deposition in an Antarctic coastal environment (Marian Cove, King George Island): Seasonal patterns from a sediment trap study. Estuarine, Coastal and Self Science, Vol. 73. p. 111-122.

Lamy, F., Ruhlemann, C., Hebbeln, D., Wefer, G., 2002. High and low-latitude climate control on the position of the southern Peru-Chile Current during the Holocene. Paleoceanography, Vol. 17, p. 1028.

Leventer, A., Domack, E., Dunbar, R., Pike, J., Stickley, C., Maddison, E., Brachfeld, S., Manley, P., McClennen, C., 2006. Marine sediment record from the East Antarctic margin reveals dynamics of ice sheet recession. Geological Society of America Today, Vol. 12, p. 4-10.

Leventer, A., personal oral communication, March 2012 (Colgate University).

Lonne, I., 1995. Sedimentary facies and depositional architecture of ice-contact glaciomarine systems. Sedimentary Geology, Vol. 98, p. 13-43.

Mercer, J.H., 1978. West Antarctic ice sheet and CO_2 greenhouse effect: a threat of disaster. Nature, Vol. 271, p. 321-325.

Michalchuck, B.R., Anderson, J.B., Wellner, J.S., Manley, P.L., Majewski, W., Bohaty, S., 2009. Holocene climate and glacial history of the northeaster Antarctic Peninsula: the marine sedimentary record from a long SHALDRIL core. Quaternary Science Reviews, Vol. 28, p. 3049-3065.

Milliken, K.T., Anderson, J.B., Wellner, J.S., Bohaty, S.M., and Manley, P.L., 2009. High-resolution Holocene climate record from Maxwell Bay, South Shetland Islands, Antarctica. Geological Society of America Bulletin, Vol. 121, p. 1711-1725.

Mosola, A.B. and Anderson, J.B., 2006. Expansion and rapid retreat of the West Antarctic Ice Sheet in eastern Ross Sea: possible consequences of over-extended ice-streams? Quaternary Science Reviews, Vol. 25, p. 2177-2196.

Pritchard, H.D., and Vaughan, D.G., 2007. Widespread acceleration of tidewater glaciers on the Antarctic Peninsula. Journal of Geophysical Research, Vol. 112, F03S29, doi: 10.1029/2006JF000597.

Pritchard, H.D., Arthern, R.J., Vaughan, D.G., Edwards, L.A., 2009. Extensive dynamic thinning on the margins of the Greenland and Antarctic ice sheets. Nature, Vol. 461, p. 971-975, doi: 10.1038/nature08471.

Pudsey, C.J. and Evans, J., 2001. First survey of Antarctic sub-ice shelf sediments reveals mid-Holocene ice shelf retreat. Geology, Vol. 29, p. 787-790.

Remy, F., and Parrenin, F., 2004. Snow accumulation variability and random walk: How to interpret changes of surface elevation in Antarctica. Earth and Planetary Science Letters, Vol. 227, p. 273-280, doi:10.1016/j.epsl.2004.09.003.

Rignot, E., Bamber, J.L., Van den Broeke, M., Davis, C., Li, Y., Van de Berg, W.J., Van Meijgaard, E., 2008. Recent Antarctic ice mass loss from radar interferometry and regional climate modeling. Nature Geoscience, Vol. 1, p. 106-110.

Rodriguez, J., Jimenez-Gomez, F., Blanco, J.M., Figueroa, F.L., 2002. Physical gradients and spatial variability of the size structure and composition of phytoplankton in the Gerlache Strait (Antarctica). Deep-Sea Research II, Vol. 49, p. 693-706.

Rosenheim, B.E., Day, M.B., Domack, E., Schrum, H., Benthien, A., Hayes, J.M., 2008. Antarctic sediment chronology by programmed-temperature pyrolysis: Methodology and data treatment. Geochemistry Geophysics Geosystems, Vol. 9, doi:10.1029/2007GC001816.

Rundle, A.S., 1973. Glaciology of the Maar Ice Piedmont, Anvers Island, Antarctica. Ohio State University Institute of Polar Studies Report, Vol. 47, p. 237.

Scambos, T., Hulbe, C., Fahnestock, M., 2003. Climate-induced ice shelf disintegration in the Antarctic Peninsula. Paliobiology and Paleoenvironments of Eoscene rocks, Antarctic Research Series, Vol. 76, p. 335-347.

Shipboard Scientific Party, 2005, SHALDRIL 2005 Cruise Report, p. 189.

Shipboard Scientific Party, 2007, NBP0703 2007 Cruise Report Summary, p. 52.

Simms, A.R., Milliken, K.T., Anderson, J.B., Wellner, J.S., 2011. The marine record of deglaciation of the South Shetland Islands, Antarctica since the Last Glacial Maximum. Quaternary Science Reviews, Vol. 30, p. 1583-1601.

Stuiver, M., and Reimer, P.J., 1993. Extended ^{14}C database and revised CALIB radiocarbon calibration program. Radiocarbon, Vol. 35, p. 215-230.

Szczucinski, W., and Zajaczkowski, M., 2012. Factors controlling downward fluxes of particulate matter in glacier-contact and non-glacier contact settings in a subpolar fjord (Billefjorden, Svalbard). International Association of Sedimentology Special Publications, Vol. 44, p. 369-386.

Thomas, E.R., Marshall, G.J., McConnell, J.R., 2008. A doubling in snow accumulation in the western Antarctic Peninsula since 1850. Geophysical Research Letters, Vol. 35, L01706, doi: 10.1029/2007GL032529.

Vaughan, D.G., Marshall., G.J., Connolley, W.M., Parkinson, C., Mulvaney, R., Hodgson, D.A., King, J.C., Pudsey, C.J., Turner, J., 2003. Recent rapid regional climate warming on the Antarctic Peninsula. Climate Change, Vol. 60, p. 243-274.

Wellner, J.S., Lowe, A.L., Shipp, S.S., Anderson, J.B., 2001. Distribution of glacial geomorphic features on the Antarctic continental shelf and correlation with substrate; implications for ice behavior. Journal of Glaciology, Vol. 47, p. 397-411.

Wellner, J.S., Heroy, D.C., Anderson, J.B., 2006. The death mask of the Antarctic ice sheet: Comparison of glacial geomorphic features across the continental shelf. Geomorphology, Vol. 75, p. 157-171.

Wentworth, C.K., 1922. A scale of grade and class terms for clastic sediments. The Journal of Geology, Vol. 30, p. 377-392.

Appendix 1: Core Data

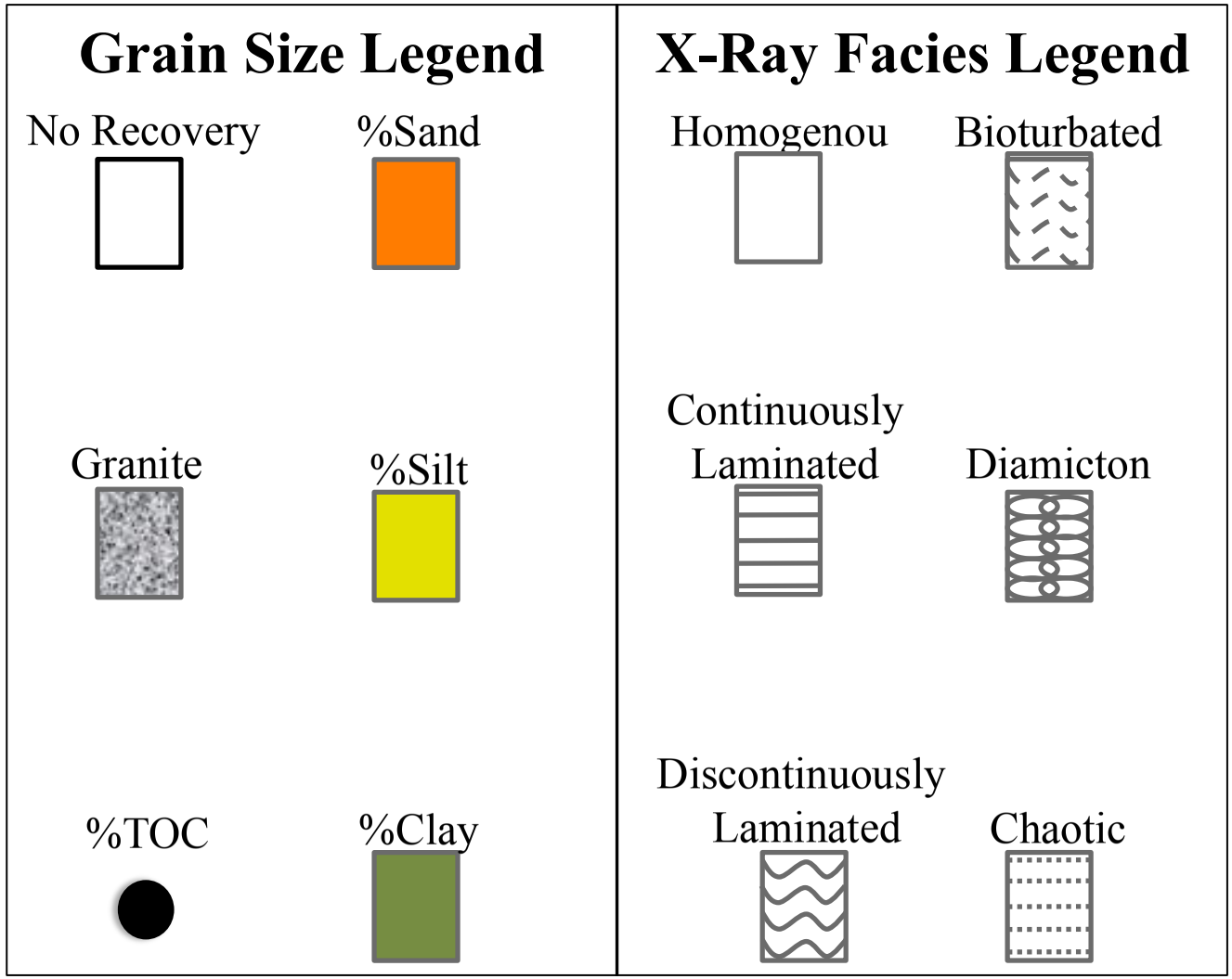

Figure A1-1. Legend for x-ray facies, and grain size analysis.

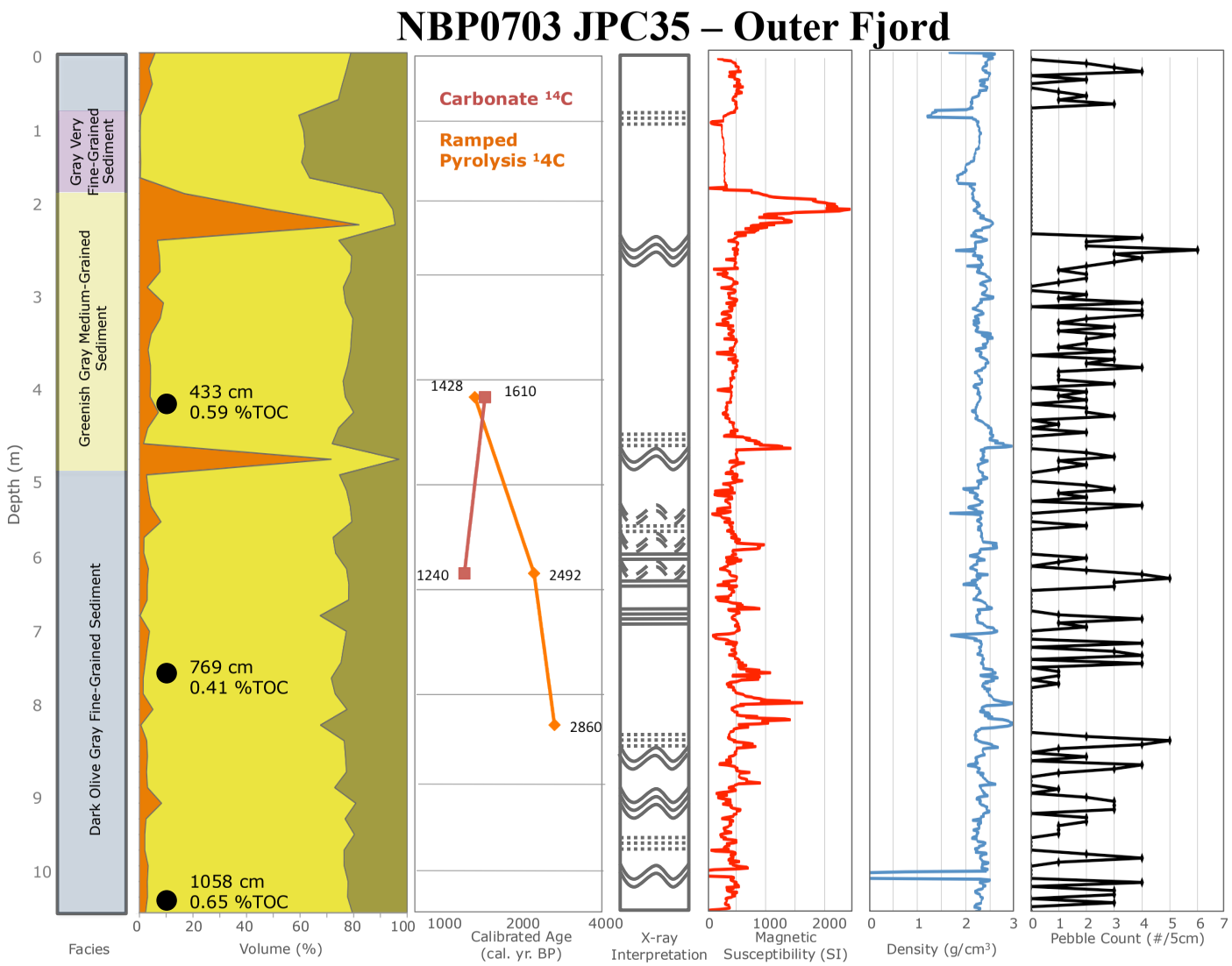

Figure A1-2. Core data for NBP0703 JPC35.

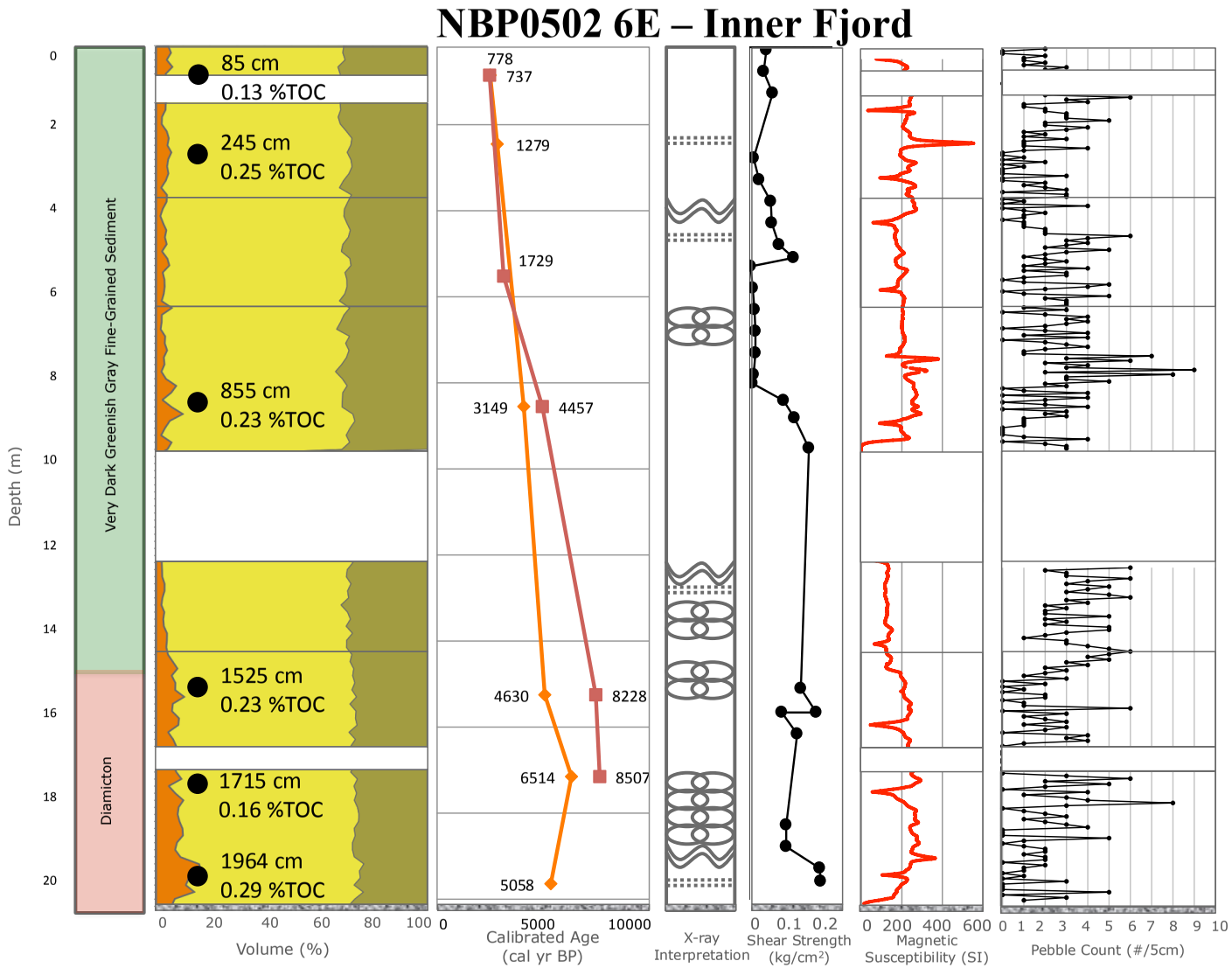

Figure A1-3. Core data for NBP0703 JPC35.

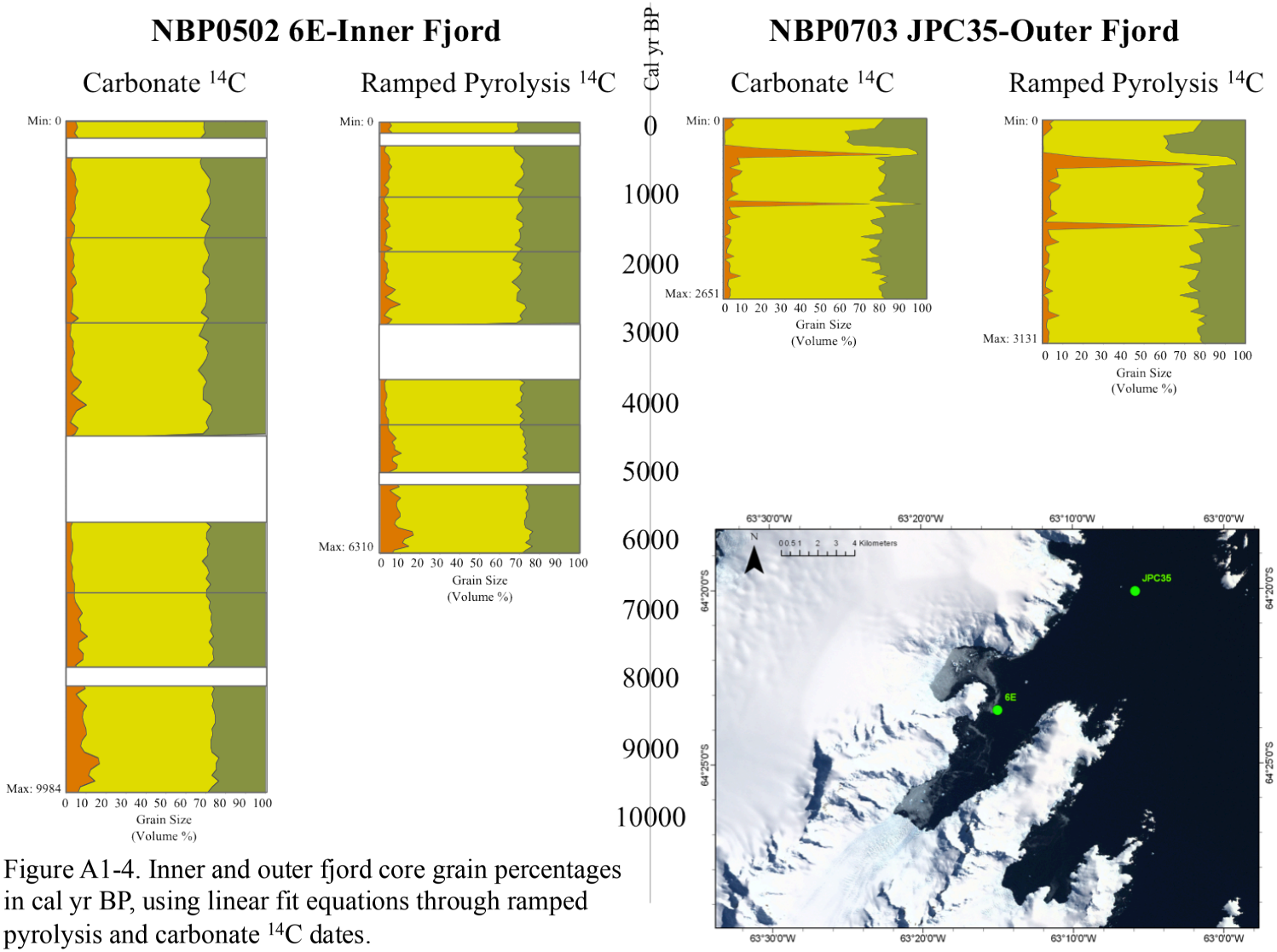

Figure A1-4. Inner and outer fjord core grain percentages in cal yr BP, using linear fit equations through ramped pyrolysis and carbonate ^{14}C dates.

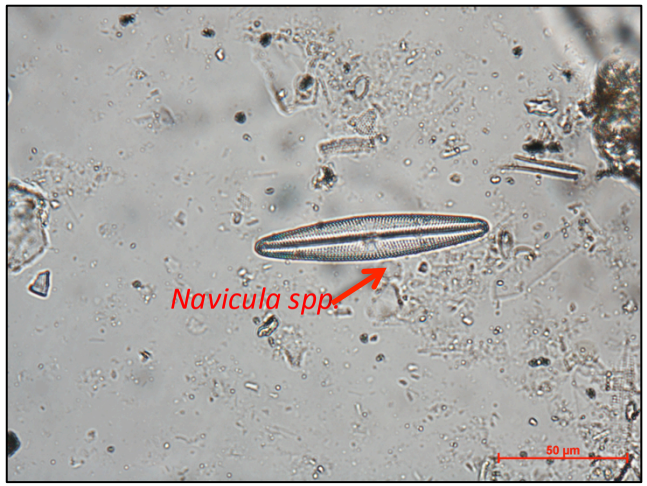

NBP0703 JPC35 489 cm

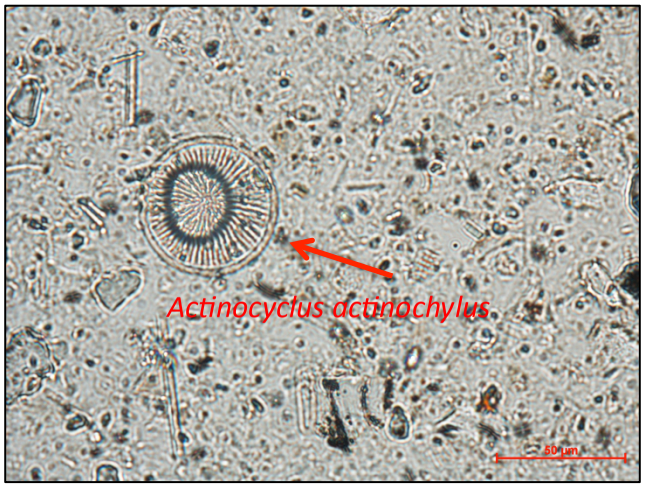

NBP0703 JPC35 769 cm

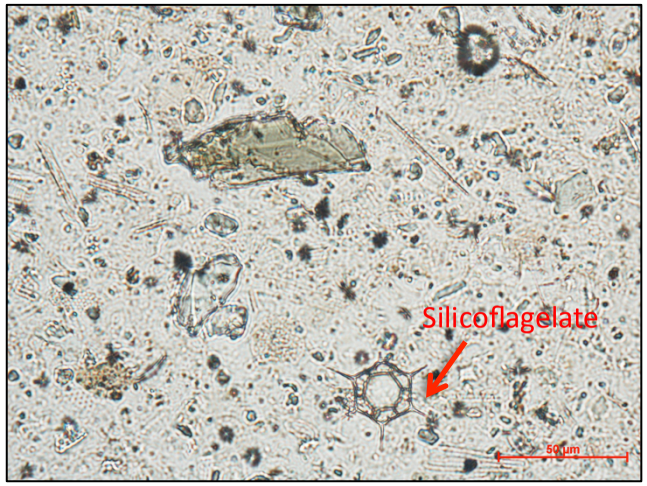

NBP0703 JPC35 769 cm

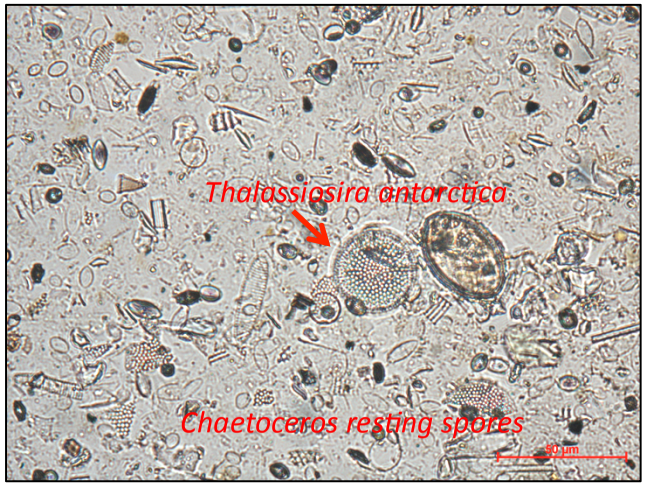

NBP0703 JPC35 920 cm

Figure A1-5. Additional smear slides from NBP0703 JPC35.

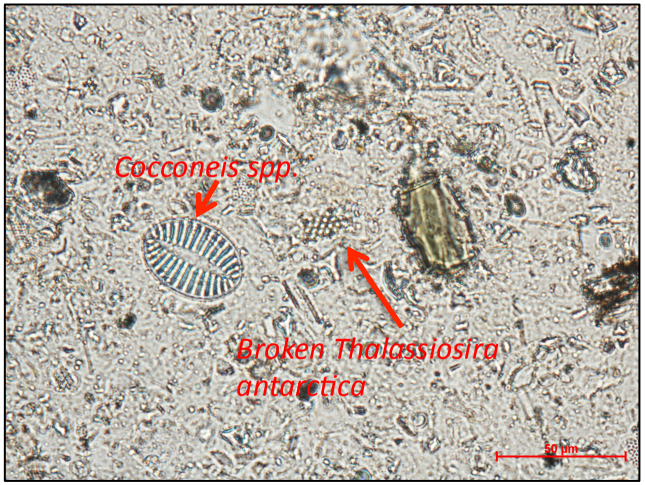

NBP0502 6E 245 cm

NBP0502 6E 1425 cm

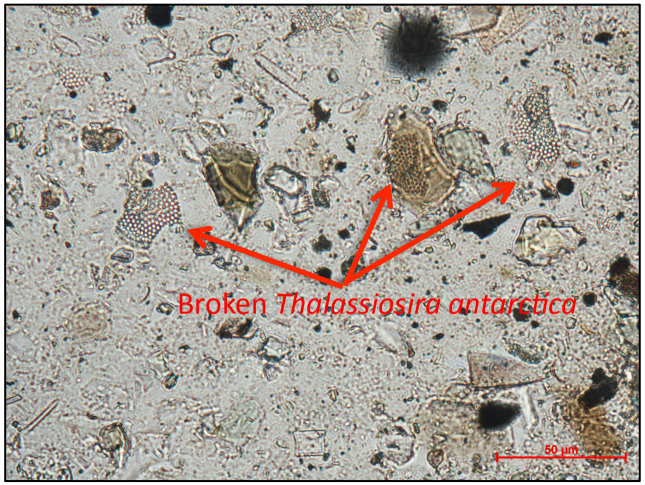

NBP0502 6E 1796 cm

Figure A1-6. Additional smear slides from NBP0502 6E.

Appendix 2: Chronology Results

Lab Number	Core	Depth (cm)	Uncalibrated (^{14}C yrs BP)	Lab Error	Cal yr BP	Age Error
58871	NBP0703 JPC35	433	2740	0.0043	1610	50
105508	NBP0703 JPC35	768	4030	0.0077	1240	110
83299	NBP0502 6D	45	1865	0.0031	708	35
69383	NBP0502 6E	85	1900	0.0029	737	30
83300	NBP0502 6D	185	2525	0.0036	1364	40
83301	NBP0502 6D	265	2530	0.0071	1381	80
83302	NBP0502 6D	285	2675	0.0039	1532	45
83298	NBP0502 6E	552	2840	0.0132	1729	160
40847	NBP0502 6E	855	5025	0.0015	4457	35
69382	NBP0502 6E	1525	8460	0.0093	8228	220
105509	NBP0502 6E	1715	10280	0.0195	8507	570

Table A2-1.Carbonate radiocarbon results, with uncalibrated dates for comparison to other studies. For calibration, an 1100 year reservoir was applied (Milliken et al., 2009). Calibration was conducted using Calib 6.0 software through the Marine09 curve.

Sample Pyrolysis Code	Aliquot Interval	Core	Depth (cm)	$T_{minimum}$ (°C)	$T_{maximum}$ (°C)	Photometric CO_2 (µmol)	Uncalibrated (^{14}C yrs BP)
DB-116-20110513	116_1	NBP0502 6E	85	ambient	318	5.02	1970
DB-116-20110513	116_2	NBP0502 6E	85	318	367	5.25	1930
DB-116-20110513	116_3	NBP0502 6E	85	367	431	6.49	2150
DB-116-20110513	116_4	NBP0502 6E	85	431	489	5.58	2080
DB-116-20110513	116_5	NBP0502 6E	85	489	698	10.26	2660
DB-122-20110517	122_1	NBP0502 6E	245	ambient	323	10.98	2430
DB-122-20110517	122_2	NBP0502 6E	245	323	377	8.68	2530
DB-122-20110517	122_3	NBP0502 6E	245	377	424	6.88	2900
DB-122-20110517	122_4	NBP0502 6E	245	424	499	9.51	2770
DB-122-20110517	122_5	NBP0502 6E	245	499	701	12.25	2840
DB-117-20110513	117_1	NBP0502 6E	855	ambient	303	5.06	4000
DB-117-20110513	117_2	NBP0502 6E	855	303	361	7.08	4250
DB-117-20110513	117_3	NBP0502 6E	855	361	419	6.81	4370
DB-117-20110513	117_4	NBP0502 6E	855	419	483	7.17	4370
DB-117-20110513	117_5	NBP0502 6E	855	483	692	14.2	4450
DB-118-20110514	118_1	NBP0502 6E	1525	ambient	325	5.25	5160
DB-118-20110514	118_2	NBP0502 6E	1525	325	382	5.94	6100
DB-118-20110514	118_3	NBP0502 6E	1525	382	438	5.70	6730
DB-118-20110514	118_4	NBP0502 6E	1525	438	516	7.93	6120
DB-118-20110514	118_5	NBP0502 6E	1525	516	697	9.87	5900

Table A2-2.All ramped pyrolysis samples sent to National Ocean Sciences Accelerator Mass Spectrometry Facility (NOSAMS). Highlighted samples are the youngest aliquot ages for a particular horizon, and are therefore used as the true age of the sample.

Sample Pyrolysis Code	Aliquot Interval	Core	Depth (cm)	$T_{minimum}$ (°C)	$T_{maximum}$ (°C)	Photometric CO_2 (µmol)	Uncalibrated (^{14}C yrs BP)
DB-112-20110511	112_1	NBP0502 6E	1715	ambient	349	5.72	6790
DB-112-20110511	112_2	NBP0502 6E	1715	349	463	8.17	8430
DB-112-20110511	112_3	NBP0502 6E	1715	463	577	8.88	7740
DB-112-20110511	112_4	NBP0502 6E	1715	577	750	3.65	8420
DB-113-20110511	113_1	NBP0502 6E	1964	ambient	330	5.02	5480
DB-113-20110511	113_2	NBP0502 6E	1964	330	392	5.01	7420
DB-113-20110511	113_3	NBP0502 6E	1964	392	464	5.95	8190
DB-113-20110511	113_4	NBP0502 6E	1964	464	558	8.91	6970
DB-113-20110511	113_5	NBP0502 6E	1964	558	763	6.49	7940
DB-124-20110518	124_1	NBP0703 JPC35	433	ambient	301	6.06	2590
DB-124-20110518	124_2	NBP0703 JPC35	433	301	359	8.58	2580
DB-124-20110518	124_3	NBP0703 JPC35	433	359	407	7.71	2900
DB-124-20110518	124_4	NBP0703 JPC35	433	407	462	7.86	2720
DB-124-20110518	124_5	NBP0703 JPC35	433	462	702	20.50	2950
DB-120-20110516	120_1	NBP0703 JPC35	769	ambient	294	5.39	3450
DB-120-20110516	120_2	NBP0703 JPC35	769	294	351	8.63	3450
DB-120-20110516	120_3	NBP0703 JPC35	769	351	402	7.71	3680
DB-120-20110516	120_4	NBP0703 JPC35	769	402	468	9.55	3900
DB-120-20110516	120_5	NBP0703 JPC35	769	468	718	19.42	3840
DB-121-20110516	121_1	NBP0703 JPC35	1058	ambient	308	7.51	3750

Table A2-2 continued.

Sample Pyrolysis Code	Aliquot Interval	Core	Depth (cm)	$T_{minimum}$ (°C)	$T_{maximum}$ (°C)	Photometric CO_2 (µmol)	Uncalibrated (^{14}C yrs BP)
DB-121-20110516	121_2	NBP0703 JPC35	1058	308	349	6.21	3910
DB-121-20110516	121_3	NBP0703 JPC35	1058	349	410	9.05	4260
DB-121-20110516	121_4	NBP0703 JPC35	1058	410	481	10.13	4310
DB-121-20110516	121_5	NBP0703 JPC35	1058	481	700	19.79	4270

Table A2-2 continued.

Lab Number	Core	Depth (cm)	Uncalibrated (^{14}C yrs BP)	Lab Error	Cal yr BP	Age Error
88517	NBP0502 6E	85	1930	0.0026	778	25
88538	NBP0502 6E	245	2430	0.0053	1279	55
88519	NBP0502 6E	855	4000	0.0019	3149	25
88523	NBP0502 6E	1525	5160	0.0047	4630	70
88504	NBP0502 6E	1715	6790	0.0047	6514	85
88508	NBP0502 6E	1964	5480	0.0057	5058	90
88544	NBP0703 JPC35	433	2580	0.0059	1428	65
88529	NBP0703 JPC35	769	3450	0.0026	2492	35
88533	NBP0703 JPC35	1058	3750	0.006	2860	75

Table A2-3.Ramped pyrolysis radiocarbon results and calibration for the youngest dated aliquot of each horizon sampled. Uncalibrated dates included for comparison to other studies. For calibration, an 1100 year reservoir was applied (Milliken et al., 2009). Calibration was conducted using Calib 6.0 software through the Marine09 curve.

	NBP0502 6E (Inner Fjord)	**NBP0502 6E *with 6D* (Inner Fjord)**	**NBP0703 JPC 35 (Outer Fjord)**
Raw Ramped Pyrolysis ^{14}C Method	~ 2.1 mm/yr	~ 2.1 mm/yr	~ 2.4 mm/yr
Calibrated Ramped Pyrolysis ^{14}C Method	~ 2.6 mm/yr	~ 2.6 mm/yr	~ 3.3 mm/yr
Raw Carbonate ^{14}C Method	~ 1.5 mm/yr	~ 1.2 mm/yr	~ 1.7 mm/yr
Calibrated Carbonate ^{14}C Method	~ 2.0 mm/yr	~1.8 mm/yr	~ 4.4 mm/yr

Table A2-4. Average sedimentation rates calculated from both dating methods for the inner and outer fjord cores. Raw and calibrated rates are recorded for comparison to other studies. NBP0502 6E and NBP0502 6D cores were collected adjacently, so dates from each are used to construct the age profile and average sedimentation rate of the inner fjord.

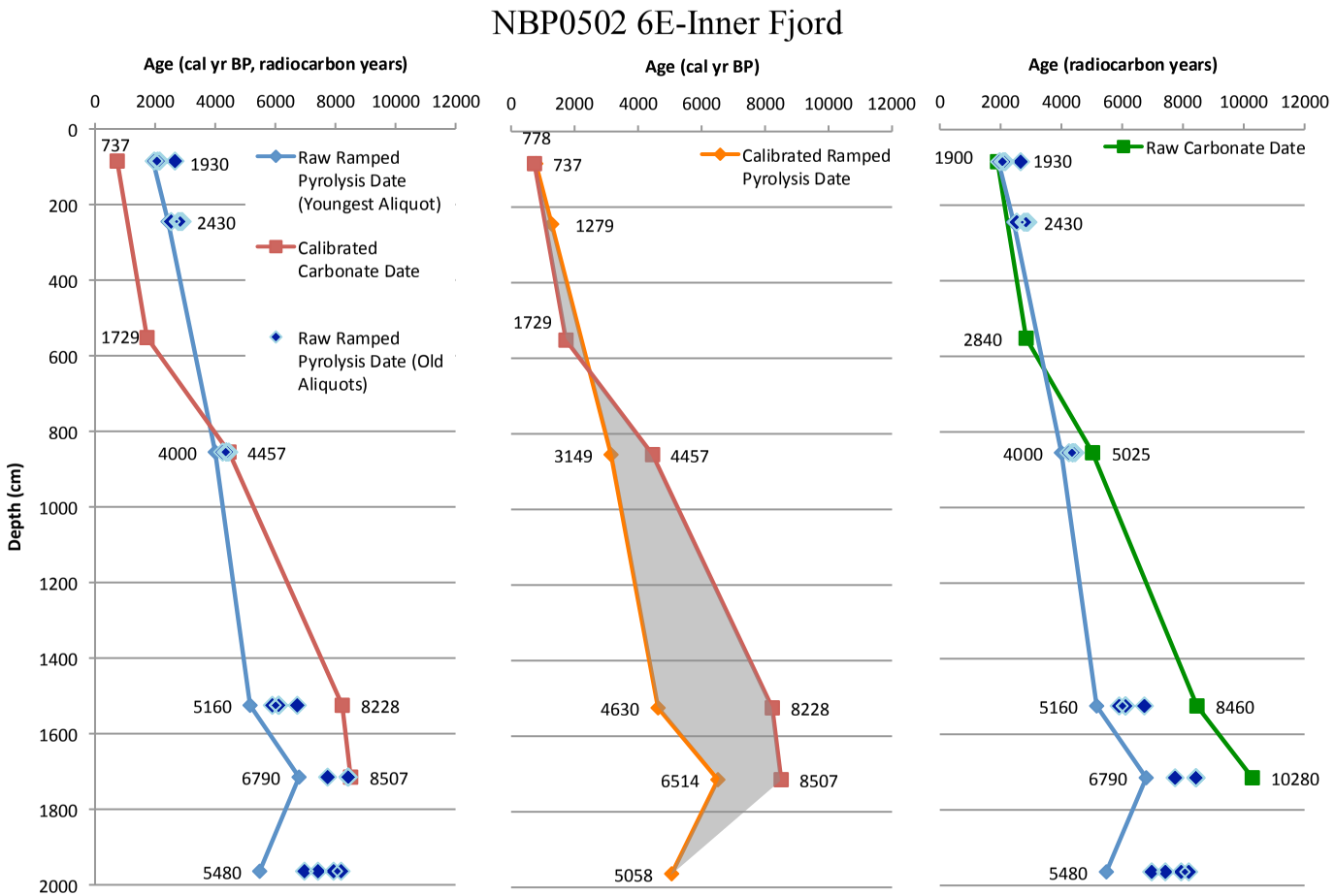

Figure A2-1. NBP0502 6E uncalibrated and calibrated ramped pyrolysis ^{14}C dates compared to carbonate ^{14}C dates. Raw ramped pyrolysis youngest aliquot ages (true ages) are plotted with older aliquot ages from the same horizons, as the variability in aliquot ages indicates how heterogeneously aged organic carbon is within the sediment. Gray area in the center calibrated/calibrated graph represents the offset between both dating methods.

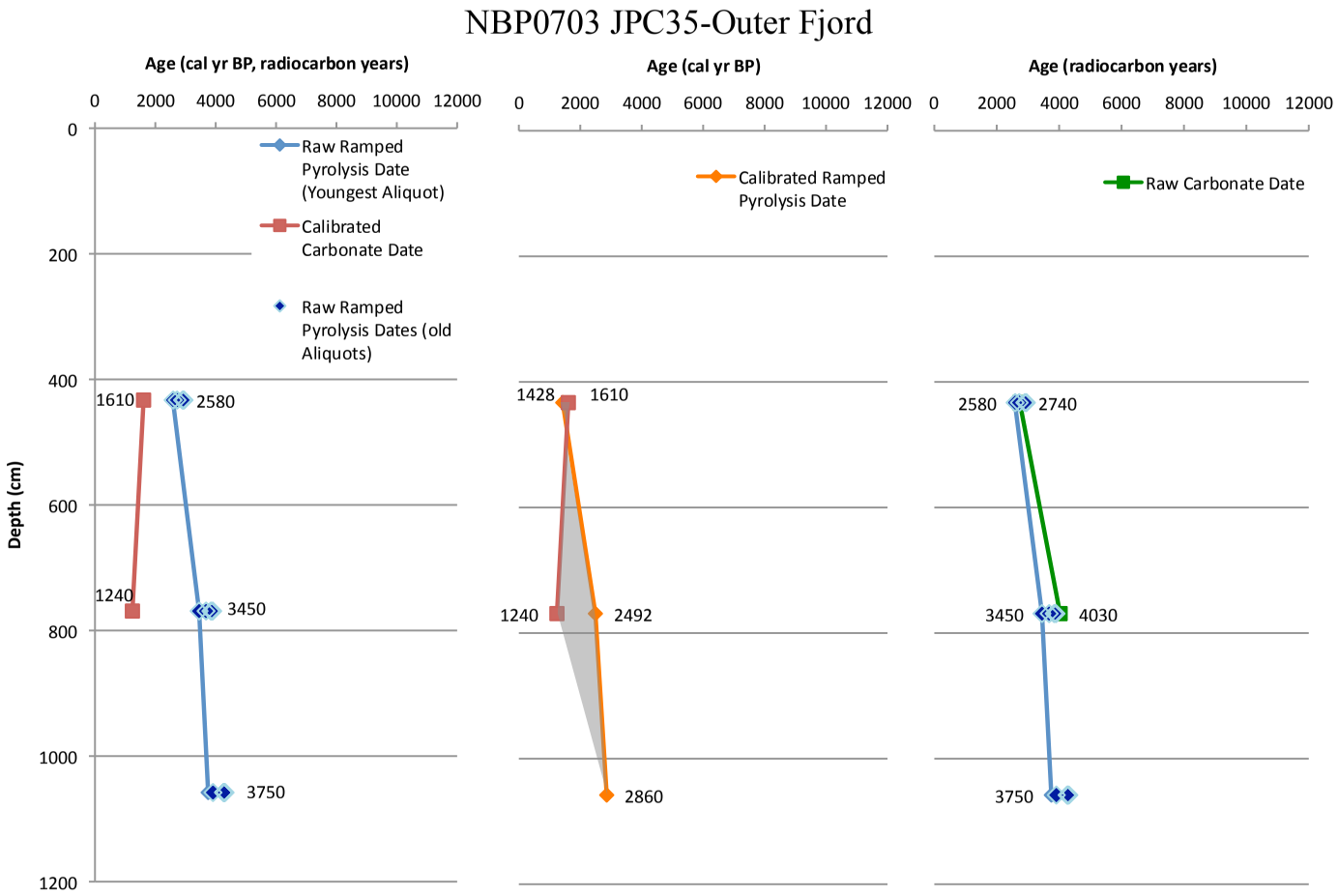

Figure A2-2. NBP0703 JPC-35 uncalibrated and calibrated ramped pyrolysis ^{14}C dates compared to carbonate ^{14}C dates. Raw ramped pyrolysis youngest aliquot ages (true ages) are plotted with older aliquot ages from the same horizons, as the variability in aliquot ages indicates how heterogeneously aged organic carbon is within the sediment. Gray area in the center calibrated/calibrated graph represents the offset between both dating methods.

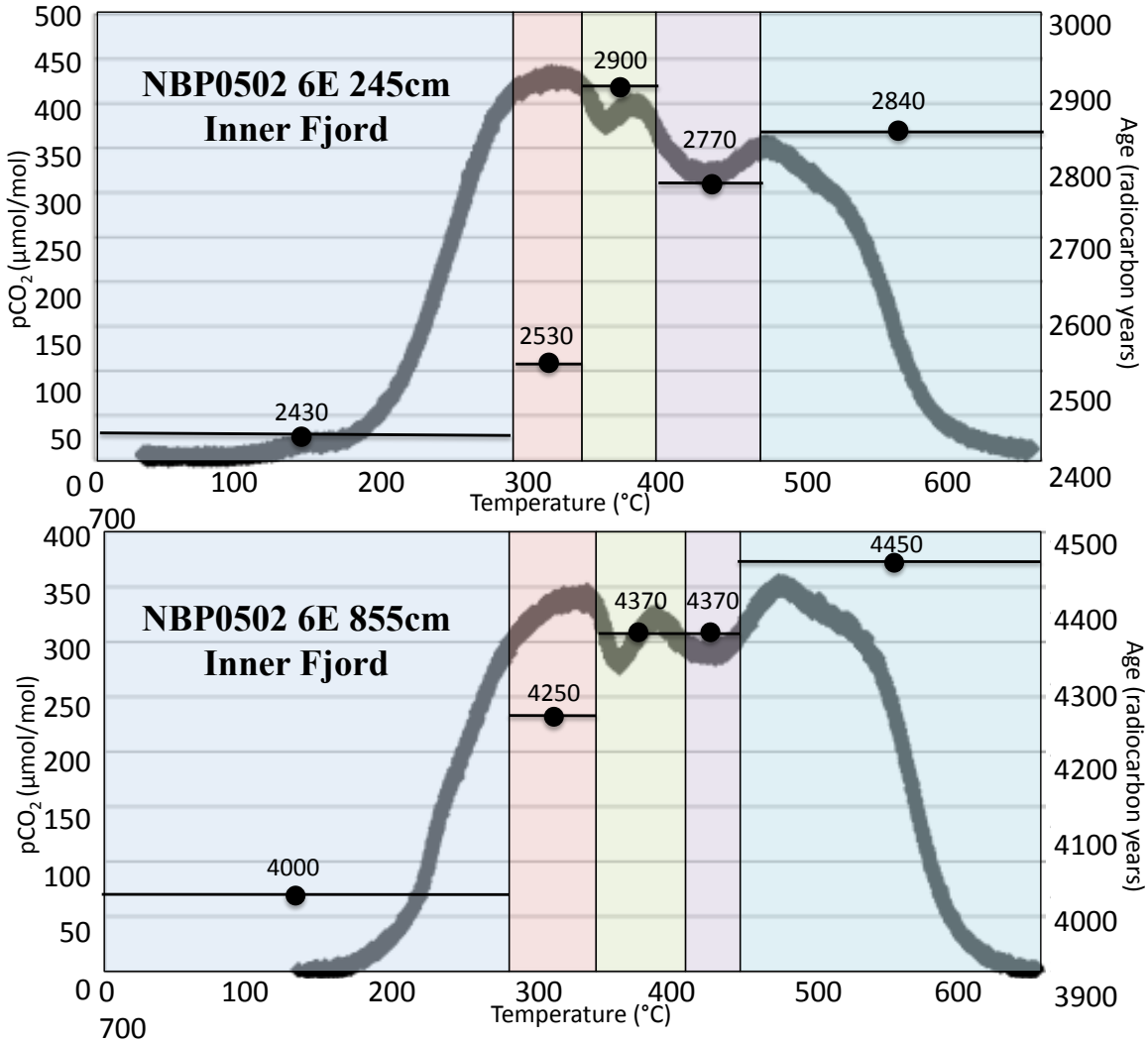

Figure A2-3. Ramped pyrolysis thermographs from two NBP0502 6E depths, each with five gas aliquots sampled. Bar height indicates age of aliquot trapped over a temperature range (bar width). Photometrically measured CO_2 is also noted on the left axis as measured on the heavy black line. In each case the youngest aliquot date was used as the true age of the sample.